HHS Public Access

Author manuscript

Neuron. Author manuscript; available in PMC 2017 September 21.

Published in final edited form as:

Neuron. 2016 September 21; 91(6): 1356–1373. doi:10.1016/j.neuron.2016.08.009.

Modulating neuronal competition dynamics in the dentate gyrus to rejuvenate aging memory circuits

Kathleen M. McAvoy[1,2,3], **Kimberly N. Scobie**[4], **Stefan Berger**[5], **Craig Russo**[1,2], **Nannan Guo**[1,2,3], **Pakanat Decharatanachart**[1], **Hugo-Vega Ramirez**[1,2,3], **Sam Miake-Lye**[1], **Michael Whalen**[6], **Mark Nelson**[7], **Matteo Bergami**[8], **Dusan Bartsch**[5], **Rene Hen**[4], **Benedikt Berninger**[9], and **Amar Sahay**[1,2,3]

[1]Center for Regenerative Medicine, Massachusetts General Hospital, Boston, MA 02114, USA

[2]Harvard Stem Cell Institute, Cambridge, MA 02138, USA

[3]Department of Psychiatry, Massachusetts General Hospital, Harvard Medical School, Boston, MA 02114 USA

[4]Departments of Neuroscience and Psychiatry, Columbia University, NY, USA

[5]Department of Molecular Biology, Central Institute of Mental Health and Medical Faculty Mannheim, Heidelberg University, 68159, Mannheim, Germany

[6]Neuroscience Center, Massachusetts General Hospital, Boston, MA 02129, USA

[7]Echelon Biosciences, Salt lake City, Utah

[8]Cologne Excellence Cluster on Cellular Stress Responses in Aging-Associated Diseases (CECAD) and University Hospital of Cologne, Joseph-Stelzmann-Straβe 26, D-50931 Cologne, Germany

[9]Institute of Physiological Chemistry, University Medical Center Johannes Gutenberg University, Mainz, Germany

SUMMARY

The neural circuit mechanisms underlying the integration and functions of adult-born dentate granule cell (DGCs) are poorly understood. Adult-born DGCs are thought to compete with mature DGCs for inputs to integrate. Transient genetic overexpression of a negative regulator of dendritic spines, Kruppel-like factor 9 (Klf9), in mature DGCs enhanced integration of adult-born DGCs and increased NSC activation. Reversal of Klf9 overexpression in mature DGCs restored spines, activity, and reset neuronal competition dynamics and NSC activation, leaving the DG modified by

*Correspondence: Amar Sahay (asahay@mgh.harvard.edu).

AUTHOR CONTRIBUTIONS

K.M, C.R, N.G, P.D, H.R, and S.M-L performed experiments. K.N.S, S.B, R.H, M.B, B.B, M.N, D.B contributed reagents and shared resources. A.S and K.M co-developed the concept, analyzed data and wrote the manuscript. A.S conceived the project and supervised all aspects of the project.

a functionally integrated, expanded cohort of age-matched adult-born DGCs. Spine elimination by inducible deletion of Rac1 in mature DGCs increased survival of adult-born DGCs without affecting proliferation or DGC activity. Enhanced integration of adult-born DGCs transiently reorganized adult-born DGC local afferent connectivity and promoted global remapping in the DG. Rejuvenation of the DG by enhancing integration of adult-born DGCs in adulthood, middle age and aging enhanced memory precision.

Graphical Abstract

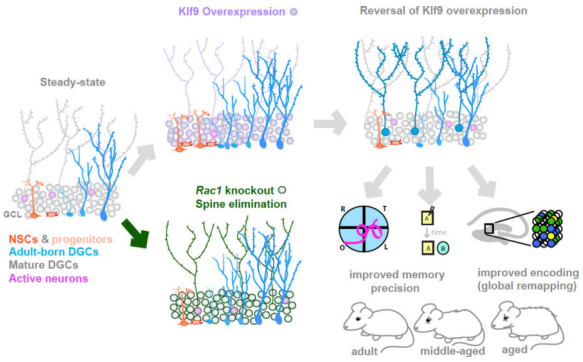

INTRODUCTION

Neural stem cells (NSCs) in the dentate gyrus (DG) sub-region of the hippocampus generate dentate granule cells (DGCs) throughout life, with substantial turnover of the DG reported in humans (Altman and Das, 1965; Eriksson et al., 1998; Spalding et al., 2013). Considerable evidence suggests that levels of adult hippocampal neurogenesis are highly sensitive to experience (Kempermann et al., 1997; van Praag et al., 2000), indicating that neurogenesis is dynamically regulated by circuit demands. It has been suggested that adult-born DGCs must compete with mature DGCs for entorhinal cortical inputs in order to integrate into the hippocampal circuit. Anatomical studies show that maturing adult-born DGCs first form synapses onto pre-existing perforant path-DGC synapses, before establishing monosynaptic connections with those perforant path terminals (Toni et al., 2007). Deletion of the N-Methyl-D-aspartate (NMDA) receptor in 2–3 weeks old adult-born DGCs impairs their survival, indicating a role for activity in integration of adult-born DGCs (Tashiro et al., 2006). These observations raise the possibility that mature DGC input connectivity dictates the dynamics of adult-born DGC competition.

Studies interrogating functional contributions of adult hippocampal neurogenesis support a role for adult-born DGCs in resolving interference between competing goals or overlapping contextual or spatial information (Wojtowicz et al., 2008; Clelland et al., 2009; Garthe et al., 2009; Tronel et al., 2010; Sahay et al., 2011a; Burghardt et al., 2012; Nakashiba et al., 2012; Niibori et al., 2012; Pan et al., 2012; Vukovic et al., 2013; Swan et al., 2014; Besnard and Sahay, 2015). Aging is accompanied by numerous changes in the hippocampus associated with impairments in resolution of interference (Toner et al., 2009; Yassa et al., 2011; Yassa and Stark, 2011; Gracian et al., 2013; Wu et al., 2015). Whether enhancing adult

hippocampal neurogenesis in middle age or during aging improves memory functions is not known.

One neural mechanism by which interference between similar memories in the DG-CA3 circuit is decreased is through pattern separation, a process by which similar inputs are made more distinct during storage (McNaughton and Morris, 1987; O'Reilly and McClelland, 1994; Gilbert et al., 2001; Rolls and Kesner, 2006; Bakker et al., 2008). In the DG, this computational process may be mediated by encoding inputs in non-overlapping ensembles of neurons (global remapping) (Leutgeb et al., 2007; Deng et al., 2013; Neunuebel and Knierim, 2014). Whether adult neurogenesis promotes network-level mechanisms underlying pattern separation in the DG is not known.

To begin to bridge these gaps in our understanding, we engineered a genetic system to inducibly and reversibly overexpress a negative transcriptional regulator of dendritic spines, Kruppel-like factor 9 (Klf9) in mature DGCs. Overexpression of Klf9 eliminated a subset of dendritic spines of mature DGCs, decreased their activity, and robustly enhanced integration of adult-born DGCs and activation of NSCs without affecting olfactory bulb neurogenesis. Independently targeting *Rac1* to eliminate spines in mature DGCs likewise promoted the integration of adult-born DGCs. Restoration of *Klf9* expression to physiological levels restored dendritic spines and reverted levels of neurogenesis to steady state, while modifying the DG with an integrated, expanded population of adult-born DGCs. Adult mice with an expanded cohort of 5–8 week-old adult-born DGCs showed improved cognitive flexibility, memory precision, and long-term contextual memory, whereas rejuvenating the DG during aging improved memory precision. Expanding the population of 5–8 week-old adult-born DGCs enhanced global remapping in the DG, causally linking adult hippocampal neurogenesis with network-level mechanisms supporting pattern separation in the DG.

RESULTS

A genetic system for inducible and reversible overexpression of *Klf9* in mature DGCs

To determine the impact of modulating dendritic spines of mature DGCs on neuronal competition dynamics and NSC activation, we developed a genetic system to reversibly eliminate dendritic spines of mature DGCs in the adult hippocampus. As previous work suggests that Klf9 functions as a negative regulator of dendritic spines of hippocampal neurons *in vitro* and *in vivo* (Scobie et al., 2009)(unpublished observations), without affecting neuronal survival, we hypothesized that *Klf9* overexpression in mature DGCs would decrease their dendritic spine density. We generated a tetO-Klf9 knock-in mouse line to permit reversible induction of *Klf9* expression *in vivo*. tetO-Klf9 knock-in mice exhibit comparable *Klf9* expression to wild-type mice (data not shown) and were bred with a CaMKII rtTA driver sub-line to generate bigenic CaMKII rtTA; tetO-Klf9/tetO-Klf9 mice (hereafter $mDG^{K/K}$ mice)(Figure 1A–C). We selected this CaMKII rtTA driver line based on robust induction of three independent tetO-linked transgenes in mature, but not immature Doublecortin-positive (DCX+) DGCs <3wks of age (Snyder et al., 2009), by 2 weeks of 9-tert-butyl-doxycycline (9TBD) treatment (Figure 1F–G, S1C–F). Further, we found using a tetO-H2B GFP reporter line (Foudi et al., 2009) that rtTA transactivates H2B–GFP expression in 39.13±8.59% of 4-week-old adult-born cells and 60.86±8.62% of 6-week-old

adult-born cells. Adult *mDG*$^{K/K}$ mice showed significant elevation of levels of *Klf9* transcripts in the DG-GCL (but not hilar cells), CA3, CA1, and piriform cortex, after 2 weeks of 9TBD treatment (Figure 1D–E; S1A–B, t-test, vehicle vs. 9TBD, DG p<0.0001, CA3 p=0.0152, CA1 p<0.0001, PC p=0.0004). Critically, *Klf9* overexpression reverted to baseline levels following a two week-long "chase" period (Figure 1D–E; S1B).

Reversible overexpression of *Klf9* in mature DGCs transiently decreases their dendritic spine density and activity

To determine the effect of *Klf9* overexpression on dendritic spine density, we bred *mDG*$^{K/K}$ mice with Thy-1 GFP (M line) mice in which GFP is expressed in DGCs >6wks of age (Figure 2A–B) (Vuksic et al., 2008). Induction of *Klf9* overexpression in *mDG*$^{K/K;Thy\_1GFP}$ *mice* decreased spine density in the outer molecular layer (OML) of the DG (t-test, vehicle vs. 9TBD, dorsal p=0.0074, ventral p=0.0067) and stratum radiatum (SR) of dorsal CA1 (t-test, vehicle vs. 9TBD, p=0.0264) without affecting spine density in the inner molecular layer (IML) of the DG (Figure 2C–D, S2F, immediate timepoint). *Klf9* overexpression likely decreased functional spines, as *mDG*$^{K/K;Thy\_1GFP}$ mice also showed a reduction in the density of PSD95-containing spines in the OML (t-test, vehicle vs. 9TBD, p=0.0095) (Figure 2G); however, *Klf9* overexpression did not change the distribution of dendritic spine size in the DG or CA1 (Figure 2E–F) or size distribution of mossy fiber terminals of mature DGCs (Figure 2H). Reversal of *Klf9* overexpression restored spine density at the chase timepoint (Figure 2C–D). This restoration is unlikely to be due to homeostatic changes since 4 weeks of *Klf9* overexpression in mDG$^{K/K}$ mice maintained dendritic spine loss in the DG (Figure 3K, data not shown). Analysis of cleaved caspase-3+ cells in the GCL of vehicle and 9TBD treated mDG$^{K/K}$ mice detected negligible caspase activation, indicating that *Klf9* overexpression and the reduction in mature DGC spine density does not cause cell death (Figure S2H).

Klf9 overexpression (immediate timepoint) resulted in a significant decrease in activity of DG, CA3, and CA1 at baseline (home cage, t-test, vehicle vs. 9TBD, DG p=0.0353, CA3 p=0.0446, CA1 p=0.0242) and following exploration of an open field (Figure 2I, S2A–B) (t-test, vehicle vs. 9TBD, DG p=0.0092, CA3 p=0.0269, CA1 p=0.0488). Reversal of *Klf9* overexpression (chase timepoint) restored neuronal activation (Figure 2J, S2C–D) in parallel with the restoration of dendritic spine density in DG-OML and CA1-SR. 9TBD and vehicle-treated mDG$^{K/K}$ mice also showed comparable spine densities of striatal and retrosplenial cortical neurons at the chase time point (Figure S2 E , G). Thus, inducible *Klf9* overexpression negatively regulates dendritic spine density and activity of mature DGCs *in vivo*.

Reversible overexpression of *Klf9* in mature DGCs modulates neuronal competition dynamics and activation of NSCs

We next addressed the impact of decreasing mature DGC dendritic spines and activity on neuronal competition dynamics and NSC activation. 9TBD-treated *mDG*$^{K/K}$ mice showed a 1.8±0.07-fold increase (t-test, vehicle vs. 9TBD, p=0.0028) in the DCX+ population at the immediate timepoint, and this enhancement in DCX+ numbers reverted back to steady-state levels at the chase timepoint (Figure 3A–C). The enhancement in the DCX+ population was

dependent on both genotype and treatment (Figure S3C) and limited to the DG, with no affect on SVZ neurogenesis (Figure S3E–G). Importantly, the transient enhancement in the DCX+ population translated into a 1.86±0.19-fold increase (t-test, vehicle vs. 9TBD, p=0.0118) in survival of mature (5-week-old) adult-born DGCs following restoration of *Klf9*, thereby modifying the DG with an expanded cohort of surviving age-matched adult-born DGCs (Figure 3A–B, F, S3A–B). Cell-fate specification in this surviving population (79.5±5.1% NeuN+) was unaffected by *Klf9* overexpression in mature DGCs (Figure S4A–B).

To ascertain the age of adult-born DGCs whose survival was impacted by *Klf9* overexpression in mature DGCs, we labeled dividing cells at multiple timepoints prior to, and during, 9TBD treatment of $mDG^{K/K}$ mice (Figure S3A). We found that the survival of ~2–3-week-old, but not 3–4-week-old, adult-born cells was enhanced by *Klf9* overexpression in mature DGCs (Figure S3A,B,D), consistent with previous reports suggesting a critical window for activity dependent integration (Tashiro et al., 2006). In addition, the population of cells born one week into the course of 9TBD treatment was also expanded (data not shown). These data suggest that a 2 week induction-2 week chase protocol enables expansion of a cohort of 3–6-week-old adult-born DGCs.

To further probe the relationship between dendritic spines of mature DGCs and adult hippocampal neurogenesis, we analyzed the DCX+ population in $mDG^{K/K;Thy1\text{-}GFP}$ mice in which we quantified mature DGC spine density (Figure 2C,D). We found that the size of the DCX+ adult-born DGC population is inversely correlated with spine density of mature DGCs (vehicle: n=9, Spearman $r = -0.6193$, p=0.0497; 9TBD: n=14, Spearman $r = -0.6879$, p=0.0082, combined groups: Spearman r=-0.7540, p<0.0001, Figure 3K).

Interestingly, *Klf9* overexpression in mature DGCs also increased activation of NSCs and progenitors (Figure 3A, B, D, E, G-J). At the immediate timepoint, 9TBD-treated $mDG^{K/K}$ mice exhibited significant increases in activation of NSCs and progenitors expressing mini-chromosome maintenance factor 2 (MCM2, a marker of cell cycle and G0 to early G1 transition, t-test, vehicle vs. 9TBD, IMM p=0.0048) or Tbr2 (t-test, vehicle vs. 9TBD, p=0.0023, Figure 3A,D-E). We also saw a significant increase in activated type I NSCs [(Nestin-expressing cells with radial-glial–like morphology that co-express MCM2, (Figure 3G–H, t-test, vehicle vs. 9TBD, p=0.0001)]. In addition, we bred Nestin-GFP mice with $mDG^{K/K}$ mice and observed an increase in GFP+ type I cells that also expressed MCM2 (Figure 3I–J, t-test, vehicle vs. 9TBD, p=0.0219). Furthermore, the 3.37±0.38 fold enhancement in NSC activation is transient and returns to basal levels following a two-week chase (Figure 3H).

We next asked whether we could repeatedly enhance neurogenesis in $mDG^{K/K}$ mice. We found that a second treatment with 9TBD 56 days following the first induction induced *Klf9* overexpression, activation of NSCs, and expansion of the population of adult-born DGCs to similar extent as that seen following a single treatment of 9TBD (Figure S6F–L). Thus, $mDG^{K/K}$ mice can be used to modify the DG with expanded populations of age-matched adult-born DGCs over multiple timepoints in the animal's lifetime.

Conditional elimination of *Rac1* in mature DGCs decreases spine density and increases the survival of adult-born DGCs

To independently determine if dendritic spine elimination in mature DGCs dictates integration of adult-born DGCs, we designed a strategy to acutely delete the Rho family GTPase Rac1, a cytoskeletal regulator of spines, in a small population of mature DGCs (Tada and Sheng, 2006)(Figure 4A). We injected the upper blade of the dorsal DG in $Rac1^{f/f}$ mice and $Rac1^{+/+}$ littermates with AAV viruses expressing Cre and conditional eYFP or eGFP to infect a small population of mature DGCs (DCX-, data not shown). Three weeks following infection, we found that acute elimination of *Rac1* decreased mature DGC OML spine density (Figure 4 B,C, t-test, control vs. Rac1, p=0.0101) without affecting activity (Figure 4B,F). Analysis of the density of DCX+ cells revealed a small but significant increase in the DCX+ population within the zone of mature DGCs with reduced dendritic spines (i='inside' the region of viral expression, o='outside' corresponding region on the contralateral section; One-way ANOVA, F=5.617, p=0.0058, n=7,5, con. i vs. con. o: ns, con. i vs. Rac1 i: p<0.05, Rac1 o vs. Rac1 i: p<0.05). Within this sample, there was a larger increase in the DCX+ population with secondary and tertiary dendrites (One-way ANOVA, F=12.2, p<0.0001, n=7,5, con. i vs. con. o: ns, con. i vs. Rac1 i: p<0.05, Rac1 o vs. Rac1 i: p<0.05; fold increase total DCX 1.42±0.12, fold increase 2–3 DCX 2.33±0.31 t-test p=0.0241, Figure 4 B , D). However, elimination of *Rac1* did not affect the size of the dividing population expressing MCM2 (Figure 4 B , E). These observations strongly suggest that reduction of mature DGC spine density is sufficient to promote expansion of the integrating DCX+ population.

Genetic enhancement of adult hippocampal neurogenesis transiently reorganizes local afferent connectivity of maturing adult-born DGCs

To understand how the topographic organization of inputs to adult-born DGCs is modified by enhancing their integration, we employed retroviral labeling and pseudo-typed rabies virus trans-synaptic tracing (Wickersham et al., 2007; Vivar et al., 2012; Deshpande et al., 2013; Bergami et al., 2015). Infection with modified rabies virus (ENV-A pseudotyped RABV lacking G glycoprotein and expressing GFP, SADΔG-GFP, Figure 5E) (Wickersham et al., 2007) is restricted to a specific, labeled population of starter cells expressing the avian receptor TVA, and limits tracing to first-order pre-synaptic partners, as further trans-synaptic is abrogated in the absence of G. Here, we injected retroviruses expressing DsRed-2A–G-IRES-TVA into dorsal DG of $mDG^{K/K}$ mice prior to treatment with vehicle or 9TBD, followed by DG injections of RABV (SADΔG-GFP) 3 or 5 weeks following retroviral infection. Mice were sacrificed one week post-RABV infection (Figure 5E). We did not see a difference in the general morphology of the 4 and 6-week-old adult-born DGCs from vehicle and 9-TBD-treated mice (Figure S4 F - I), nor did we see a difference in size or number of MFT-filopodia of 5-week-old DGCs labeled with retrovirus expressing tdTomato (Figure S4C–E). However, 4-week-old, but not 6-week-old, adult-born DGCs of 9TBD treated $mDG^{K/K}$ mice showed a significant increase in dendritic spine density in the OML (Figure 5A–D, t-test, 4wk vehicle vs. 9TBD, p<0.0001). We observed inputs from local (DG hilus, GCL, and ML) interneurons (INs) and mossy cells, CA3 interneurons and long-range projections from neurons of the medial septum and entorhinal cortex (EC) (Vivar et al., 2012; Deshpande et al., 2013; Bergami et al., 2015; Vivar et al., 2016). Using location,

morphology, and marker expression (data not shown) the GFP-only positive presynaptic neurons within the DG were identified as glutamatergic hilar mossy cells or distinct types of GABAergic interneurons distributed between the hilus (e.g., HIPP cells), the SGZ)/GCL (e.g., basket cells, HICAP cells) and the molecular layer (ML; e.g., MOPP and axo-axonic cells). 4-week-old adult-born DGCs of 9TBD treated $mDG^{K/K}$ mice had a significantly lower connectivity ratio (t-test, vehicle vs. 9TBD, p=0.0262) that appears to be driven by decreased connectivity with mossy cells (t-test, vehicle vs. 9TBD, p=0.03) and DG INs (t-test, vehicle vs. 9TBD, p=0.0505, Figure 5G–H). In contrast, 6-week-old adult-born DGCs in vehicle and 9TBD-treated $mDG^{K/K}$ mice exhibited similar connectivity ratios (Figure 5G–H). We did not see a difference between vehicle and 9TBD-treated mice in the relative proportions of afferent inputs from each identified region (Figure 5I). Thus, the expanded cohort of adult-born DGCs in $mDG^{K/K}$ mice show equivalent afferent synaptic connectivity upon maturation.

Genetic expansion of a cohort of 5–8-week-old adult-born DGCs decreased spatial interference and enhanced long-term memory strength and precision

Loss-of-function and electrophysiological studies support a critical role for 4–8-week-old adult-born DGCs in memory processing (Snyder et al., 2001; Schmidt-Hieber et al., 2004; Saxe et al., 2006; Ge et al., 2007; Denny et al., 2011; Gu et al., 2012; Marin-Burgin et al., 2012). To assess the impact of expanding a cohort of 5–8-week-old adult-born DGCs on hippocampal-dependent memory functions, we extended the chase period following *Klf9* overexpression to 4 weeks before starting behavioral testing. 9TBD treated adult mice showed normal innate anxiety, behavioral despair, and modestly improved novel object recognition memory (Figure S5A–F). Both vehicle and 9TBD-treated adult mice located the hidden platform in the morris water maze with comparable latencies (ANOVA, day: $F_{(8,144)}$=33.52, p<0.0001, treatment: $F_{(1,18)}$=0.1187, p=0.7344, interaction: $F_{(8,144)}$=0.6848, p=0.8016) and swim speed (data not shown) during the acquisition phase (days 1–9) and preferred the target quadrant during the first probe trial on day 10 (Figure 6A–C) (ANOVA, vehicle: F=3.46, p=0.0262, target v left, opposite p<0.05, 9TBD: F=8.4, p=0.0002, target v left, right, opposite p<0.05). We then assessed reversal spatial learning by switching the platform location to the opposite quadrant. Both vehicle and 9TBD treated $mDG^{K/K}$ mice showed similar latencies to reach the platform in the new location (ANOVA, day: $F_{(4,72)}$=14.43, p<0.0001, treatment: $F_{(1,18)}$=1.492, p=0.2376, interaction: $F_{(4,72)}$=0.8749, p=0.4833, Figure 6D). However, in a probe trial on day 3 of the reversal phase, only the mice with an expanded cohort of 5–8 week adult-born neurons preferred the new target location (Figure 6E, ANOVA, vehicle: F=0.64, p=0.5942, 9TBD: F=5.97, p=0.0021, target v left, right, opposite p<0.05), while the control group perseverated in the original target location, only acquiring the same level of performance with three additional days of training (Figure 6F, ANOVA, vehicle: F=313.79, p<0.0001, target v left, right, opposite p<0.05, 9TBD: F=9.166, p=0.0001, target v left, right, opposite p<0.05). In a separate series of experiments, we found that mice with reversible overexpression of *Klf9* only in CA1 showed no improvement in cognitive flexibility in the reversal learning task (Figure S5 J - Q).

Using a behaviorally naïve cohort of adult $mDG^{K/K}$ mice, we examined the effect of expanding the cohort of 5–8 week adult-born DGCs on contextual fear discrimination

memory. While both groups of mice showed comparable acquisition of contextual fear learning on days 1–3 (ANOVA, day: $F_{(2,38)}$=34.66, p<0.0001, treatment: $F_{(1,19)}$=1.997, p=0.2732, interaction: $F_{(2.38)}$=1.053, p=0.3590) and contextual fear discrimination on day 4 (ANOVA A vs. B, context: $F_{(1,19)}$= 42.71, p<0.0001, treatment: $F_{(1,19)}$= 0.1384, p=0.714, interaction: $F_{(1,19)}$=2.606, p=0.123; t-test, A vs. B, vehicle: p=0.0352, 9TBD: p=0.0006, ANOVA A vs. C, context: $F_{(1,19)}$= 58.99, p<0.0001, treatment: $F_{(1,19)}$= 0.8742, p=0.3615, interaction: $F_{(1,19)}$=0.7341, p=0.4022; t-test, A vs. C, vehicle: p<0.0001, 9TBD: p<0.0001) and 2 weeks post-training (ANOVA, context: $F_{(1,19)}$= 18.18, p=0.004, treatment: $F_{(1,19)}$= 2.494, p=0.1308, interaction: $F_{(1,19)}$=0.0061, p=0.9384; t-test, A vs. B, vehicle: p=0.0333, 9TBD: p=0.0209), the mice with more 5–8-week-old adult-born DGCs exhibited modestly stronger contextual fear memory and context discrimination 4 weeks post-training (ANOVA, context: $F_{(1,19)}$= 1.834, p=0.0213, treatment: $F_{(1,19)}$= 4.152, p=0.0558, interaction: $F_{(1,19)}$=2.048, p=0.1686; t-test, A vs. B, 9TBD: p=0.0546; vehicle A vs. 9TBD A: p=0.0495, Figure 6J–L).

To determine whether these cognitive improvements were due to increased adult hippocampal neurogenesis and not other processes such as reversible spine elimination, we utilized a pharmacological strategy (Garthe et al., 2009; Akers et al., 2014) to occlude the enhancement in neurogenesis in 9TBD treated $mDG^{K/K}$ mice. Administration of saline (vehicle) or temozolomide (TMZ, i.p. 3x /week), a DNA alkylating agent that causes cell death of dividing cells, to adult $mDG^{K/K}$ mice prior to and during sucrose or 9TBD treatment (Figure 6G) blocked enhancement of DG neurogenesis and significantly reduced SVZ neurogenesis (t-test, n=4,5, vehicle/sucrose vs. TMZ/9TBD DG p=0.1862, SVZ p=0.0105) (Figure 6H, I). Utilizing this treatment, followed by a four-week chase, period both vehicle/sucrose and TMZ/9TBD-treated groups showed comparable acquisition of contextual fear learning (ANOVA, day: $F_{(2,32)}$= 61.26, p<0.0001, treatment: $F_{(1,16)}$= 0.8728 , p=0.3641, interaction: $F_{(2,32)}$=1.025, p=0.3703, Figure 6K) and comparable contextual fear discrimination on day 4 (ANOVA, context: $F_{(1,16)}$= 45.86, p<0.0001, treatment: $F_{(1,16)}$= 0.0737, p=0.7895, interaction: $F_{(1,16)}$=0.2951, p=0.5945; t-test, A vs. B, vehicle/sucrose: p<0.0001, TMZ/9TBD: p=0.0013), and at 2 weeks post-training (ANOVA, context: $F_{(1,16)}$= 49.11, p<0.0001, treatment: $F_{(1,16)}$=1.629, p=0.2213, interaction: $F_{(1,16)}$=0.0075, p=0.9319; t-test, A vs. B, vehicle: p=0.0482, 9TBD: p=0.0198). Neither group showed discrimination at 4 weeks post training (Figure 6M).

Contextual memory precision is improved in middle-aged and aged mice with expanded populations of 5–8 -week-old adult-born DGCs

Analysis of Klf9 transcripts in 9TBD-treated 11 and 17-month-old $mDG^{K/K}$ mice showed a robust elevation in *Klf9* levels in the DG but not CA3 or CA1 (Figure S6A–B, 7m data not shown). Immediately following two weeks of 9TBD treatment middle-aged and aged $mDG^{K/K}$ mice showed a significant expansion in the DCX+ population (vehicle vs. 9TBD t-test, 11m p=0.0137, 5.9±1.11-fold increase; 17m, vehicle vs. 9TBD p=0.0004, 7.63±0.88-fold increase) and ~2 fold increase in survival in 3-week-old cells (Figure 7A, B, D, E, t-test, 11mos., vehicle vs. 9TBD p=0.0004; t-test, 17mos., vehicle vs. 9TBD p=0.0441). Additionally, in middle-aged and aged mice *Klf9* overexpression in mature DGCs robustly activated NSCs (Figure 7A, C, t-test vehicle vs. 9TBD, middle-aged p=0.0277; aged

p<0.0001) and in middle aged mice increased the number of Tbr2+ (5.5±0.24 fold increase) and MCM2+ cells (3.6±0.22 fold increase, Figure S6C–E). Importantly, these observations suggest that we can rejuvenate the DG of middle-aged and aged mice with adult-born DGCs to match the size of the adult-born DGC population in ~5–6-month-old mice (Figure 7B).

We next sought to examine the effects of expanding a cohort of 5–8-week-old adult-born DGCs in middle-aged and aged mice on contextual fear discrimination (Figure 7F–H). 12-month-old 9TBD and vehicle-treated *mDG*$^{K/K}$ mice showed comparable acquisition of contextual fear learning (ANOVA, day: $F_{(1,16)}$=0.0028, p<0.0001, treatment: $F_{(1,16)}$=50.54, p=0.3050, interaction: $F_{(1,16)}$=0.9218, p=0.4969), but the 9TBD group, unlike the controls, discriminated between the similar contexts A and B at days 4 (ANOVA, context: $F_{(1,16)}$= 50.54, p<0.0001, treatment: $F_{(1,16)}$= 0.0029, p=0.958, interaction: $F_{(1,16)}$=0.9218, p=0.3513; t-test, A vs. B, 9TBD: p=0.0002), 18 (ANOVA, context: $F_{(1,16)}$= 15.44, p=0.001, treatment: $F_{(1,16)}$= 0.0687, p=0.7963, interaction: $F_{(1,16)}$=1.980, p=0.1764; t-test, A vs. B, 9TBD: p=0.0096), and 32 (ANOVA, context: $F_{(1,16)}$= 2.404, p=0.1384, treatment: $F_{(1,16)}$= 0.0072, p=0.9333, interaction: $F_{(1,16)}$=2.526, p=0.1294; t-test, A vs. B, 9TBD: p=0.0274). In contrast, both groups discriminated between the training context A and the distinct context C at day 4 (Figure 7G) (ANOVA, context: $F_{(1,16)}$= 202.4, p<0.0001, treatment: $F_{(1,16)}$= 0.1976, p=0.6626, interaction: $F_{(1,16)}$=0.2720, p=0.6091; t-test, A vs. C, vehicle, 9TBD: p<0.0001). *mDG*$^{K/K}$ mice with an expanded cohort of 5–8-week old adult-born DGCs that had been behaviorally tested in the CFC paradigm were aged to 16 months and *Klf9* overexpression in mature DGCs was re-induced to expand another population of adult-born DGCs. Prior to re-induction, all the mice were found to not have any detectable memory (freezing behavior) of the shock context (data not shown). 9TBD and vehicle-treated 17-month-old *mDG*$^{K/K}$ mice showed normal innate anxiety behavior as assessed in the open field and light-dark paradigms (Figure S5 G - I). Both groups of aged *mDG* $^{K/K}$ mice showed comparable acquisition of contextual fear learning (ANOVA, day: $F_{(2,32)}$=77.54, p<0.0001, treatment: $F_{(1,16)}$=0.5951, p=0.4517, interaction: $F_{(2,32)}$=0.2964, p=0.7455), and both groups discriminated between the training context A and the distinct context C at day 4 (Figure 7H, ANOVA, context: $F_{(1,16)}$= 124.6, p<0.0001, treatment: $F_{(1,16)}$=0.2888, p=0.5984, interaction: $F_{(1,16)}$=4.035, p=0.0617; t-test, A vs. C, vehicle: p=0.0004, 9TBD: p<0.0001). However, the 9TBD group, unlike the controls, discriminated between the similar contexts A and B at days 4 (ANOVA, context: $F_{(1,16)}$= 17.57, p=0.0007, treatment: $F_{(1,16)}$= 0.3038, p=0.5891, interaction: $F_{(1,16)}$=1.463, p=0.244; t-test, A vs. B, 9TBD: p=0.0029) and 18 (ANOVA, context: $F_{(1,16)}$= 32.62, p=0.0898, treatment: $F_{(1,16)}$= 0.2397, p=0.6311, interaction: $F_{(1,16)}$=3.022, p=0.1013; t-test, A vs. B, 9TBD: p=0.0292). Neither group discriminated between the similar contexts A and B at day 32. Together, these observations suggest that expanding the population of 5–8-week-old adult-born DGCs in middle-aged and aged mice improves contextual memory precision.

Expansion of a cohort of 5–8-week-old adult-born DGCs enhances global remapping in the DG

Because mice with expanded populations of 5–8-week-old adult-born DGCs exhibited improved behavioral discrimination under conditions of high, but not low, interference (similar but not distinct contexts), we asked whether enhancing adult hippocampal

neurogenesis affects global remapping in the DG. We utilized catFISH (cellular compartment analysis of temporal activity using fluorescence *in situ* hybridization) to visualize cellular assemblies activated in the DG by two temporally separated exposures to contexts based on nuclear and cytoplasmic localization of *c-fos* transcripts (Guzowski and Worley, 2001). Adult 9TBD and vehicle treated $mDG^{K/K}$ mice, and an additional cohort of $mDG^{K/K}$ mice treated with vehicle/sucrose and TMZ/9TBD (as in Figure 6G) were conditioned to a foot-shock in context A over 3 days followed by one of three different context exposure conditions on day 4 (A-A, A-B, A-C, Figure 8C–E,G). Analysis of activated cell assemblies in the DG of controls in the A-A condition showed significantly higher levels of reactivation (cells positive for both nuclear and cytoplasmic transcripts, i.e. % overlap) than control mice of A-C group (t-test, vehicle A-A vs. vehicle A-C, p=0.0391), but similar overlap as control mice in the A-B group (Figure 8C–D, G, S7). Further, the ventral DG showed significantly greater overlap than dorsal DG in control mice (Figure 8C–E, G, S7, t-test, vehicle dorsal vs. ventral, A-A: p=0.0009, A-B: p<0.0001, A-C: p=0.0585). In contrast to control animals, analysis of 9TBD treated $mDG^{K/K}$ mice revealed significantly less reactivation in mice exposed to A-B than A-A (t-test, 9TBD A-A vs. A-B p=0.0296). Importantly, in the high interference A-B condition, mice with expansion of the adult-born DGC population showed significantly less re-activation of DG cellular assemblies (t-test, vehicle vs. 9TBD, dorsal p=0.0063, ventral p=0.0061) than vehicle treated $mDG^{K/K}$ mice (Figure 8D, Figure S7). Notably, this decrease in reactivation was dependent on the expanded cohort of 5–8 week old adult-born neurons, as no difference in re-activation of cellular assemblies was seen between vehicle/sucrose and TMZ/9TBD treated $mDG^{K/K}$ mice (Figure 8E, Figure S7). Middle-aged 9TBD-treated $mDG^{K/K}$ mice exposed to A-B also showed significantly less re-activation of DG cellular assemblies than vehicle-treated $mDG^{K/K}$ mice (t-test, vehicle vs. 9TBD, dorsal p=0.0393; ventral p=0.0477, Figure 8F, Figure S7). By contrast, 9TBD and vehicle-treated $mDG^{K/K}$ mice exhibited similar levels of re-activation of cellular assemblies in the low interference A-C condition.

Analysis of the total populations activated by each exposure in dorsal DG of adult mice suggested that expanding the population of 5–8-week-old adult-born DGCs increased the number of cells activated by the first exposure only in A-B and A-C conditions. Furthermore, mice with more 5–8-week-old adult-born DGCs exhibited a significant reduction in the number of cells activated only by the second exposure (Figure 8C–D, G). This increase in mismatch-dependent sparseness was lost when the enhancement in neurogenesis was blocked by TMZ (Figure 8E).

DISCUSSION

Mature DGCs are well positioned to link experience and activity with the integration of adult-born DGCs because they receive the vast majority of inputs. Here, we leveraged our identification of Klf9 as a negative regulator of dendritic spines to demonstrate that reversible elimination of OML dendritic spines of mature DGCs enhances the integration of 2–3 week old adult-born DGCs. Inducible loss of Rac1 in mature DGCs also increased this population of adult-born DGCs but did not promote activation NSCs and progenitors as seen with Klf9 overexpression in mature DGCs. Because reversible Klf9 dependent spine elimination also transiently decreased activity of mature DGCs, we speculate that decreased

DGC activity might differentially engage mossy cells and hilar interneurons (Jinde et al., 2012; Song et al., 2012) or alter release of activity-dependent secreted factors (Lie et al., 2005; Ma et al., 2009) to influence NSC and progenitor activation. Alternatively, Klf9's direct transcriptional targets may include pro-neurogenic secreted factors. Our data support the hypothesis that DG neurogenesis is controlled through overlapping, yet discrete circuit mechanisms, with mature DGC spine density primarily affecting survival of integrating adult-born DGCs, and changes in activity or secretome leading to the activation of NSCs and progenitors.

Using RABV tracing in our genetic system, we found that enhancing adult hippocampal neurogenesis did not affect entorhinal cortical connectivity with 4-week-old adult-born DGCs, even though these DGCs had more spines in the OML. However, these DGCs had decreased connectivity with mossy cells and DG-INs (Figure 5J), but unaltered spine density in the IML. These findings raise the possibility that increasing neurogenesis may drive branching of pre-synaptic terminals. In addition, it is thought that mossy cells' glutamatergic and di-synaptic inhibitory inputs coordinate unsilencing of perforant path-excitatory synapses in adult-born DGCs (Vivar et al., 2012; Deshpande et al., 2013; Chancey et al., 2014). Thus, enhancing neurogenesis may induce a transient compensatory rewiring of local connectivity to constrain unsilencing of these perforant path-DGC synapses. As 6-week-old adult-born DGCs were connected to similar numbers of mossy cells and DG-INs, it appears that presynaptic connectivity ratios are scaled up during the maturation of the expanded population of DGCs to restore organization of afferent inputs. It is also possible that 4–17-day-old and 7–21-day-old adult-born DGCs differ in their ability to compete with mature DGCs, thereby affecting connectivity ratios.

In aging as in adult mice, transient *Klf9* overexpression in mature DGCs robustly enhanced survival of adult-born DGCs, whereas the relative impact on NSC activation is much greater in the aged brain, demonstrating that *Klf9* overexpression in mature DGCs overrides the inhibitory effects of NSC-cell autonomous, niche-derived, and systemic factors on NSC activation (Hattiangady and Shetty, 2008; Villeda et al., 2011; Encinas and Sierra, 2012). In contrast to adult mice, fear conditioned middle-aged and aged control mice failed to discriminate the similar context. Expanding the population of 5–8-week-old adult-born DGCs in 12 and 17 month-old mice permitted modest discrimination of similar contexts, suggesting a role for adult-born DGCs in resolution of spatial interference that continues during aging.

Expansion of the 5–8-week-old adult-born DGC population decreased the overlap between DG ensembles activated by similar contexts in adult and middle-aged mice, an effect that was reversed by pharmacological occlusion of the enhancement in neurogenesis. Interestingly, the degree of overlap in the ventral DG was greater than that of the dorsal DG, thus arguing for differences in efficiency of population-based coding along the DG's septo-temporal axis. A previous study that used *zif268* localization for catFISH analysis in middle aged rats following a task that required resolution of non-spatial information found uniform levels of global remapping along the septo-temporal axis of the DG (Satvat et al., 2011). Thus, spatial interference may be differentially processed by the dorsal and the ventral DG, much like what has been suggested for CA1 and CA3 based on differences in place cell

properties (Jung et al., 1994; Kjelstrup et al., 2008). Simultaneous assessment of population activity in the entorhinal cortex and DG was not measured in these experiments, precluding direct assessment of either input similarity or transformation into divergent outputs, which are emblematic of pattern separation (Neunuebel and Knierim, 2014). However, because the enhancements in global remapping are seen only under conditions of high contextual overlap and require expansion of the adult-born DGC pool, it is likely that these enhancements originate in the DG and are not transferred to the DG from upstream regions.

In mice with expansion of the adult-born DGC population, this decrease in overlap is driven by increased activation of the DG in the first epoch, followed by a suppression of activation in the second epoch in A-B and A-C conditions, but not in the A-A condition. These observations suggest the existence of a neurogenesis-dependent mismatch-detection mechanism that modulates activity of the DG to decrease the overlap of activated ensembles between two consecutive exposures (Burghardt et al., 2012). Interestingly, a previous study found that decreasing adult hippocampal neurogenesis impaired global remapping in CA3 and expanded the active ensemble of CA3 neurons in the second epoch (Niibori et al., 2012). It has been suggested that mature adult-born DGCs respond preferentially to inputs to which they were previously exposed to during their maturation (Tashiro et al., 2007; Aimone et al., 2011; Kropff et al., 2015). Furthermore, adult-born DGCs recruit feed-back inhibition to modulate the activity of the DG (Sahay et al., 2011b; Ikrar et al., 2013; Restivo et al., 2015; Temprana et al., 2015). Integrating these observations, we propose a model where adult-born DGCs respond to shared features across similar contexts to suppress activity of the DG and decrease the likelihood of re-activation of mature DGCs that have encode unique features of previously experienced contexts. (Figure 8H) (McAvoy et al., 2015a).

Our findings support a role for inputs onto mature DGCs in modulating adult hippocampal neurogenesis. We demonstrate that neuronal competition dynamics may be harnessed to expand the population of adult-born DGCs across the lifespan to improve memory and population-based coding mechanisms in the DG that support pattern separation. Enhancing adult hippocampal neurogenesis may have therapeutic significance in moderating impairments in pattern separation associated with aging and mild cognitive impairment (Yassa et al., 2010; Small et al., 2011; Yassa et al., 2011; Bakker et al., 2012).

METHODS

Mouse lines and animal care

Generation of TRE-Klf9 mouse line is described in Supplemental Methods. The original *CaMKIIα rtTA* line was generated as described (Zhu et al., 2007) with one of the sub-lines described in detail here. All mouse lines were housed four to five per cage in a 12 h (7:00 A.M. to 7:00P.M.) light/dark colony room at 22–24°C with ad libitum access to food and water. All animals were handled and experiments were conducted in accordance with procedures approved by the Institutional Animal Care and Use Committee at the Massachusetts General Hospital in accordance with NIH guidelines.

9-tert-butyl-doxycycline (9TBD)administration

Mice were given 2mg/mL 9TBD (Echelon Biosciences) in 3% sucrose, or 3% sucrose alone (vehicle), for 14 days in dark bottles. Solutions were freshly prepared and replaced every three days. Liquid consumption was monitored for the entire dosing period.

BrdU injections and Temozolomide (TMZ) treatment

To assess the survival of adult-born cells in the DG, BrdU was administered via intraperitoneal injection, in 0.9% NaCl at 100, 150, or 200mg/kg body weight. For injections assessing survival at multiple timepoints, CldU and IdU were injected and detected as described previously (Stone et al., 2011). Timing of each BrdU injection is described in the accompanying schematic. Mice were given 25mg/kg TMZ as described previously (Garthe et al., 2009; Akers et al., 2014). For the final two weeks of vehicle or TMZ treatment, the mice were given drinking water with sucrose (vehicle group) or 9TBD (TMZ group) as described above.

In Situ hybridization and catFISH

Klf-9 riboprobe was generated from the 3'-untranslated region of mouse *Klf-9* (NM 010638) corresponding to nucleotides 1500 –1780 as previously described (Scobie et al., 2009). For catfish experiments, animals experienced two 5-min behavioural episodes 25 min apart and brains were isolated and flash frozen in isopentane on dry ice immediately after the second episode. An intronic *c-fos* probe containing the entire first intron of the *fos* gene (Lin et al., 2011)(generous gift of Dr. Dayu Lin) and a full-length *c-fos* cRNA probe were used to detect nuclear and cytoplasmic c-fos transcripts, respectively. Nuclear *c-fos* was defined as puncta colocalizing with DAPI labeling, whereas cytoplasmic labeling was defined as *c-fos* positive dots surrounding the nucleus.

Immunohistochemistry

Mice were anaesthetized with ketamine or xylazine (100 and 2.6 mg/kg body weight, respectively) and transcardially perfused with cold saline, followed by 4% cold paraformaldehyde in PBS. Brains were postfixed overnight in 4% paraformaldehyde at 4°C, then cryoprotected in 30% sucrose and stored at 4 °C before freezing in OCT on dry ice. Coronal serial sections (35μm) were obtained using a Leica cryostat in 6 matched sets. Immunohistochemistry was performed on one set of tissue as described in the supplemental methods. Dendritic spine and mossy fiber terminal analysis was performed as described previously (McAvoy et al., 2015b).

Retroviral / Rabies virus / AAV injections

Retroviral labeling of adult-born DGCs (Ikrar et al., 2013) and rabies virus trans-synaptic tracing was performed as described previously (Deshpande et al., 2013; Bergami et al., 2015). To assess the impact of Rac1 loss, adult male Rac1 floxed (*Rac1*$^{f/f}$) or wild-type littermates (*Rac1*$^{+/+}$) were injected in dorsal DG with AAV_9-CaMKinaseIIα-Cre:GFP and AAV_5-EF1α–DIO-eYFP viruses and were sacrificed after 3 weeks.

Contextual fear conditioning and Morris water maze tasks

Behavioral assessments were performed as previously described (Sahay et al., 2011a) and are detailed in supplementary methods.

Statistical Analysis

Statistical tests were carried out as indicated in Supplemental Methods.

Supplementary Material

Refer to Web version on PubMed Central for supplementary material.

Acknowledgments

We wish to thank members of the Sahay lab for their comments on the manuscript, Dr. Dayu Lin for the c-fos plasmid and Dr. Karl-Klaus Conzelmann for the rabies virus. A.S is supported by US National Institutes of Health Biobehavioral Research Awards for Innovative New Scientists (BRAINS) 1-R01MH104175, NIH-NIA 1R01AG048908-01A1, Ellison Medical Foundation New Scholar in Aging, Whitehall Foundation, Inscopix Decode award, Ellison Family Philanthropic support, Harvard Neurodiscovery Center/MADRC Center Pilot Grant Award and HSCI Development grant. C.R and P.D were supported by HSCI Harvard Internship Program Award. We dedicate this manuscript to the late Dr. Joseph Altman who pioneered the field of adult hippocampal neurogenesis (Altman and Das, 1965).

REFERENCES

Aimone JB, Deng W, Gage FH. Resolving new memories: a critical look at the dentate gyrus, adult neurogenesis, and pattern separation. Neuron. 2011; 70:589–596. [PubMed: 21609818]

Akers KG, Martinez-Canabal A, Restivo L, Yiu AP, De Cristofaro A, Hsiang HL, Wheeler AL, Guskjolen A, Niibori Y, Shoji H, et al. Hippocampal neurogenesis regulates forgetting during adulthood and infancy. Science. 2014; 344:598–602. [PubMed: 24812394]

Altman J, Das GD. Autoradiographic and histological evidence of postnatal hippocampal neurogenesis in rats. J Comp Neurol. 1965; 124:319–335. [PubMed: 5861717]

Bakker A, Kirwan CB, Miller M, Stark CE. Pattern separation in the human hippocampal CA3 and dentate gyrus. Science. 2008; 319:1640–1642. [PubMed: 18356518]

Bakker A, Krauss GL, Albert MS, Speck CL, Jones LR, Stark CE, Yassa MA, Bassett SS, Shelton AL, Gallagher M. Reduction of hippocampal hyperactivity improves cognition in amnestic mild cognitive impairment. Neuron. 2012; 74:467–474. [PubMed: 22578498]

Bergami M, Masserdotti G, Temprana SG, Motori E, Eriksson TM, Gobel J, Yang SM, Conzelmann KK, Schinder AF, Gotz M, et al. A critical period for experience-dependent remodeling of adult-born neuron connectivity. Neuron. 2015; 85:710–717. [PubMed: 25661179]

Besnard A, Sahay A. Adult Hippocampal Neurogenesis, Fear Generalization, and Stress. Neuropsychopharmacology. 2015

Burghardt NS, Park EH, Hen R, Fenton AA. Adult-born hippocampal neurons promote cognitive flexibility in mice. Hippocampus. 2012; 22:1795–1808. [PubMed: 22431384]

Chancey JH, Poulsen DJ, Wadiche JI, Overstreet-Wadiche L. Hilar mossy cells provide the first glutamatergic synapses to adult-born dentate granule cells. J Neurosci. 2014; 34:2349–2354. [PubMed: 24501373]

Clelland CD, Choi M, Romberg C, Clemenson GD Jr, Fragniere A, Tyers P, Jessberger S, Saksida LM, Barker RA, Gage FH, et al. A functional role for adult hippocampal neurogenesis in spatial pattern separation. Science. 2009; 325:210–213. [PubMed: 19590004]

Deng W, Mayford M, Gage FH. Selection of distinct populations of dentate granule cells in response to inputs as a mechanism for pattern separation in mice. eLife. 2013; 2:e00312. [PubMed: 23538967]

Denny CA, Burghardt NSDMS, Hen R, Drew MR. 4–6 week old adult-born hippocampal neurons influence novelty-evoked exploration and contextual fear conditioning. Hippocampus. In Press. 2011

Deshpande A, Bergami M, Ghanem A, Conzelmann KK, Lepier A, Gotz M, Berninger B. Retrograde monosynaptic tracing reveals the temporal evolution of inputs onto new neurons in the adult dentate gyrus and olfactory bulb. Proc Natl Acad Sci U S A. 2013; 110:E1152–E1161. [PubMed: 23487772]

Encinas JM, Sierra A. Neural stem cell deforestation as the main force driving the age-related decline in adult hippocampal neurogenesis. Behav Brain Res. 2012; 227:433–439. [PubMed: 22019362]

Eriksson PS, Perfilieva E, Bjork-Eriksson T, Alborn AM, Nordborg C, Peterson DA, Gage FH. Neurogenesis in the adult human hippocampus. Nat Med. 1998; 4:1313–1317. [PubMed: 9809557]

Foudi A, Hochedlinger K, Van Buren D, Schindler JW, Jaenisch R, Carey V, Hock H. Analysis of histone 2B–GFP retention reveals slowly cycling hematopoietic stem cells. Nature biotechnology. 2009; 27:84–90.

Garthe A, Behr J, Kempermann G. Adult-generated hippocampal neurons allow the flexible use of spatially precise learning strategies. PLoS ONE. 2009; 4:e5464. [PubMed: 19421325]

Ge S, Yang CH, Hsu KS, Ming GL, Song H. A critical period for enhanced synaptic plasticity in newly generated neurons of the adult brain. Neuron. 2007; 54:559–566. [PubMed: 17521569]

Gilbert PE, Kesner RP, Lee I. Dissociating hippocampal subregions: double dissociation between dentate gyrus and CA1. Hippocampus. 2001; 11:626–636. [PubMed: 11811656]

Gracian EI, Shelley LE, Morris AM, Gilbert PE. Age-related changes in place learning for adjacent and separate locations. Neurobiol Aging. 2013; 34:2304–2309. [PubMed: 23618871]

Gu Y, Arruda-Carvalho M, Wang J, Janoschka SR, Josselyn SA, Frankland PW, Ge S. Optical controlling reveals time-dependent roles for adult-born dentate granule cells. Nat Neurosci. 2012; 15:1700–1706. [PubMed: 23143513]

Guzowski JF, Worley PF. Cellular compartment analysis of temporal activity by fluorescence in situ hybridization (catFISH). Current protocols in neuroscience / editorial board, Jacqueline N Crawley [et al] Chapter. 2001; 1 Unit 1 8.

Hattiangady B, Shetty AK. Aging does not alter the number or phenotype of putative stem/progenitor cells in the neurogenic region of the hippocampus. Neurobiol Aging. 2008; 29:129–147. [PubMed: 17092610]

Ikrar T, Guo N, He K, Besnard A, Levinson S, Hill A, Lee HK, Hen R, Xu X, Sahay A. Adult neurogenesis modifies excitability of the dentate gyrus. Frontiers in neural circuits. 2013; 7:204. [PubMed: 24421758]

Jinde S, Zsiros V, Jiang Z, Nakao K, Pickel J, Kohno K, Belforte JE, Nakazawa K. Hilar mossy cell degeneration causes transient dentate granule cell hyperexcitability and impaired pattern separation. Neuron. 2012; 76:1189–1200. [PubMed: 23259953]

Jung MW, Wiener SI, McNaughton BL. Comparison of spatial firing characteristics of units in dorsal and ventral hippocampus of the rat. J Neurosci. 1994; 14:7347–7356. [PubMed: 7996180]

Kempermann G, Kuhn HG, Gage FH. More hippocampal neurons in adult mice living in an enriched environment. Nature. 1997; 386:493–495. [PubMed: 9087407]

Kjelstrup KB, Solstad T, Brun VH, Hafting T, Leutgeb S, Witter MP, Moser EI, Moser MB. Finite scale of spatial representation in the hippocampus. Science. 2008; 321:140–143. [PubMed: 18599792]

Kropff E, Yang SM, Schinder AF. Dynamic role of adult-born dentate granule cells in memory processing. Curr Opin Neurobiol. 2015; 35:21–26. [PubMed: 26100379]

Leutgeb JK, Leutgeb S, Moser MB, Moser EI. Pattern separation in the dentate gyrus and CA3 of the hippocampus. Science. 2007; 315:961–966. [PubMed: 17303747]

Lie DC, Colamarino SA, Song HJ, Desire L, Mira H, Consiglio A, Lein ES, Jessberger S, Lansford H, Dearie AR, et al. Wnt signalling regulates adult hippocampal neurogenesis. Nature. 2005; 437:1370–1375. [PubMed: 16251967]

Lin D, Boyle MP, Dollar P, Lee H, Lein ES, Perona P, Anderson DJ. Functional identification of an aggression locus in the mouse hypothalamus. Nature. 2011; 470:221–226. [PubMed: 21307935]

Ma DK, Jang MH, Guo JU, Kitabatake Y, Chang ML, Pow-Anpongkul N, Flavell RA, Lu B, Ming GL, Song H. Neuronal Activity-Induced Gadd45b Promotes Epigenetic DNA Demethylation and Adult Neurogenesis. Science. 2009

Marin-Burgin A, Mongiat LA, Pardi MB, Schinder AF. Unique processing during a period of high excitation/inhibition balance in adult-born neurons. Science. 2012; 335:1238–1242. [PubMed: 22282476]

McAvoy K, Besnard A, Sahay A. Adult hippocampal neurogenesis and pattern separation in DG: a role for feedback inhibition in modulating sparseness to govern population-based coding. Frontiers in systems neuroscience. 2015a; 9:120. [PubMed: 26347621]

McAvoy K, Russo C, Kim S, Rankin G, Sahay A. Fluoxetine induces input-specific hippocampal dendritic spine remodeling along the septotemporal axis in adulthood and middle age. Hippocampus. 2015b

McNaughton B, Morris R. Hippocampal synaptic enhancement and information storage within a distributed memory system. Trends Neurosci. 1987; 10:408–415.

Nakashiba T, Cushman JD, Pelkey KA, Renaudineau S, Buhl DL, McHugh TJ, Rodriguez Barrera V, Chittajallu R, Iwamoto KS, McBain CJ, et al. Young dentate granule cells mediate pattern separation, whereas old granule cells facilitate pattern completion. Cell. 2012; 149:188–201. [PubMed: 22365813]

Neunuebel JP, Knierim JJ. CA3 retrieves coherent representations from degraded input: direct evidence for CA3 pattern completion and dentate gyrus pattern separation. Neuron. 2014; 81:416–427. [PubMed: 24462102]

Niibori Y, Yu TS, Epp JR, Akers KG, Josselyn SA, Frankland PW. Suppression of adult neurogenesis impairs population coding of similar contexts in hippocampal CA3 region. Nature communications. 2012; 3:1253.

O'Reilly RC, McClelland JL. Hippocampal conjunctive encoding, storage, and recall: avoiding a trade-off. Hippocampus. 1994; 4:661–682. [PubMed: 7704110]

Pan YW, Chan GC, Kuo CT, Storm DR, Xia Z. Inhibition of adult neurogenesis by inducible and targeted deletion of ERK5 mitogen-activated protein kinase specifically in adult neurogenic regions impairs contextual fear extinction and remote fear memory. J Neurosci. 2012; 32:6444–6455. [PubMed: 22573667]

Restivo L, Niibori Y, Mercaldo V, Josselyn SA, Frankland PW. Development of Adult-Generated Cell Connectivity with Excitatory and Inhibitory Cell Populations in the Hippocampus. J Neurosci. 2015; 35:10600–10612. [PubMed: 26203153]

Rolls ET, Kesner RP. A computational theory of hippocampal function, and empirical tests of the theory. Prog Neurobiol. 2006; 79:1–48. [PubMed: 16781044]

Sahay A, Scobie KN, Hill AS, O'Carroll CM, Kheirbek MA, Burghardt NS, Fenton AA, Dranovsky A, Hen R. Increasing adult hippocampal neurogenesis is sufficient to improve pattern separation. Nature. 2011a; 472:466–470. [PubMed: 21460835]

Sahay A, Wilson DA, Hen R. Pattern separation: a common function for new neurons in hippocampus and olfactory bulb. Neuron. 2011b; 70:582–588. [PubMed: 21609817]

Satvat E, Schmidt B, Argraves M, Marrone DF, Markus EJ. Changes in task demands alter the pattern of zif268 expression in the dentate gyrus. J Neurosci. 2011; 31:7163–7167. [PubMed: 21562279]

Saxe MD, Battaglia F, Wang JW, Malleret G, David DJ, Monckton JE, Garcia AD, Sofroniew MV, Kandel ER, Santarelli L, et al. Ablation of hippocampal neurogenesis impairs contextual fear conditioning and synaptic plasticity in the dentate gyrus. Proc Natl Acad Sci U S A. 2006; 103:17501–17506. [PubMed: 17088541]

Schmidt-Hieber C, Jonas P, Bischofberger J. Enhanced synaptic plasticity in newly generated granule cells of the adult hippocampus. Nature. 2004; 429:184–187. [PubMed: 15107864]

Scobie KN, Hall BJ, Wilke SA, Klemenhagen KC, Fujii-Kuriyama Y, Ghosh A, Hen R, Sahay A. Kruppel-like factor 9 is necessary for late-phase neuronal maturation in the developing dentate gyrus and during adult hippocampal neurogenesis. J Neurosci. 2009; 29:9875–9887. [PubMed: 19657039]

Small SA, Schobel SA, Buxton RB, Witter MP, Barnes CA. A pathophysiological framework of hippocampal dysfunction in ageing and disease. Nat Rev Neurosci. 2011; 12:585–601. [PubMed: 21897434]

Snyder JS, Choe JS, Clifford MA, Jeurling SI, Hurley P, Brown A, Kamhi JF, Cameron HA. Adult-born hippocampal neurons are more numerous, faster maturing, and more involved in behavior in rats than in mice. The Journal of neuroscience : the official journal of the Society for Neuroscience. 2009; 29:14484–14495. [PubMed: 19923282]

Snyder JS, Kee N, Wojtowicz JM. Effects of adult neurogenesis on synaptic plasticity in the rat dentate gyrus. J Neurophysiol. 2001; 85:2423–2431. [PubMed: 11387388]

Song J, Zhong C, Bonaguidi MA, Sun GJ, Hsu D, Gu Y, Meletis K, Huang ZJ, Ge S, Enikolopov G, et al. Neuronal circuitry mechanism regulating adult quiescent neural stem-cell fate decision. Nature. 2012; 489:150–154. [PubMed: 22842902]

Spalding KL, Bergmann O, Alkass K, Bernard S, Salehpour M, Huttner HB, Bostrom E, Westerlund I, Vial C, Buchholz BA, et al. Dynamics of hippocampal neurogenesis in adult humans. Cell. 2013; 153:1219–1227. [PubMed: 23746839]

Stone SS, Teixeira CM, Zaslavsky K, Wheeler AL, Martinez-Canabal A, Wang AH, Sakaguchi M, Lozano AM, Frankland PW. Functional convergence of developmentally and adult-generated granule cells in dentate gyrus circuits supporting hippocampus-dependent memory. Hippocampus. 2011; 21:1348–1362. [PubMed: 20824726]

Swan AA, Clutton JE, Chary PK, Cook SG, Liu GG, Drew MR. Characterization of the role of adult neurogenesis in touch-screen discrimination learning. Hippocampus. 2014; 24:1581–1591. [PubMed: 25074617]

Tada T, Sheng M. Molecular mechanisms of dendritic spine morphogenesis. Curr Opin Neurobiol. 2006; 16:95–101. [PubMed: 16361095]

Tashiro A, Makino H, Gage FH. Experience-specific functional modification of the dentate gyrus through adult neurogenesis: a critical period during an immature stage. J Neurosci. 2007; 27:3252–3259. [PubMed: 17376985]

Tashiro A, Sandler VM, Toni N, Zhao C, Gage FH. NMDA-receptor-mediated, cell-specific integration of new neurons in adult dentate gyrus. Nature. 2006; 442:929–933. [PubMed: 16906136]

Temprana SG, Mongiat LA, Yang SM, Trinchero MF, Alvarez DD, Kropff E, Giacomini D, Beltramone N, Lanuza GM, Schinder AF. Delayed Coupling to Feedback Inhibition during a Critical Period for the Integration of Adult-Born Granule Cells. Neuron. 2015; 85:116–130. [PubMed: 25533485]

Toner CK, Pirogovsky E, Kirwan CB, Gilbert PE. Visual object pattern separation deficits in nondemented older adults. Learning & memory (Cold Spring Harbor, NY). 2009; 16:338–342.

Toni N, Teng EM, Bushong EA, Aimone JB, Zhao C, Consiglio A, van Praag H, Martone ME, Ellisman MH, Gage FH. Synapse formation on neurons born in the adult hippocampus. Nat Neurosci. 2007; 10:727–734. [PubMed: 17486101]

Tronel S, Belnoue L, Grosjean N, Revest JM, Piazza PV, Koehl M, Abrous DN. Adult-born neurons are necessary for extended contextual discrimination. Hippocampus. 2010

van Praag H, Kempermann G, Gage FH. Neural consequences of environmental enrichment. Nat Rev Neurosci. 2000; 1:191–198. [PubMed: 11257907]

Villeda SA, Luo J, Mosher KI, Zou B, Britschgi M, Bieri G, Stan TM, Fainberg N, Ding Z, Eggel A, et al. The ageing systemic milieu negatively regulates neurogenesis and cognitive function. Nature. 2011; 477:90–94. [PubMed: 21886162]

Vivar C, Peterson BD, van Praag H. Running rewires the neuronal network of adult-born dentate granule cells. Neuroimage. 2016; 131:29–41. [PubMed: 26589333]

Vivar C, Potter MC, Choi J, Lee JY, Stringer TP, Callaway EM, Gage FH, Suh H, van Praag H. Monosynaptic inputs to new neurons in the dentate gyrus. Nature communications. 2012; 3:1107.

Vukovic J, Borlikova GG, Ruitenberg MJ, Robinson GJ, Sullivan RK, Walker TL, Bartlett PF. Immature doublecortin-positive hippocampal neurons are important for learning but not for remembering. J Neurosci. 2013; 33:6603–6613. [PubMed: 23575857]

Vuksic M, Del Turco D, Bas Orth C, Burbach GJ, Feng G, Muller CM, Schwarzacher SW, Deller T. 3D–reconstruction and functional properties of GFP-positive and GFP-negative granule cells in the fascia dentata of the Thy1-GFP mouse. Hippocampus. 2008

Wickersham IR, Lyon DC, Barnard RJ, Mori T, Finke S, Conzelmann KK, Young JA, Callaway EM. Monosynaptic restriction of transsynaptic tracing from single, genetically targeted neurons. Neuron. 2007; 53:639–647. [PubMed: 17329205]

Wojtowicz JM, Askew ML, Winocur G. The effects of running and of inhibiting adult neurogenesis on learning and memory in rats. Eur J Neurosci. 2008; 27:1494–1502. [PubMed: 18364025]

Wu MV, Luna VM, Hen R. Running rescues a fear-based contextual discrimination deficit in aged mice. Frontiers in systems neuroscience. 2015; 9:114. [PubMed: 26321926]

Yassa MA, Mattfeld AT, Stark SM, Stark CE. Age-related memory deficits linked to circuit-specific disruptions in the hippocampus. Proc Natl Acad Sci U S A. 2011; 108:8873–8878. [PubMed: 21555581]

Yassa MA, Stark CE. Pattern separation in the hippocampus. Trends Neurosci. 2011; 34:515–525. [PubMed: 21788086]

Yassa MA, Stark SM, Bakker A, Albert MS, Gallagher M, Stark CE. High-resolution structural and functional MRI of hippocampal CA3 and dentate gyrus in patients with amnestic Mild Cognitive Impairment. Neuroimage. 2010; 51:1242–1252. [PubMed: 20338246]

Zhu P, Aller MI, Baron U, Cambridge S, Bausen M, Herb J, Sawinski J, Cetin A, Osten P, Nelson ML, et al. Silencing and un-silencing of tetracycline-controlled genes in neurons. PLoS ONE. 2007; 2:e533. [PubMed: 17579707]

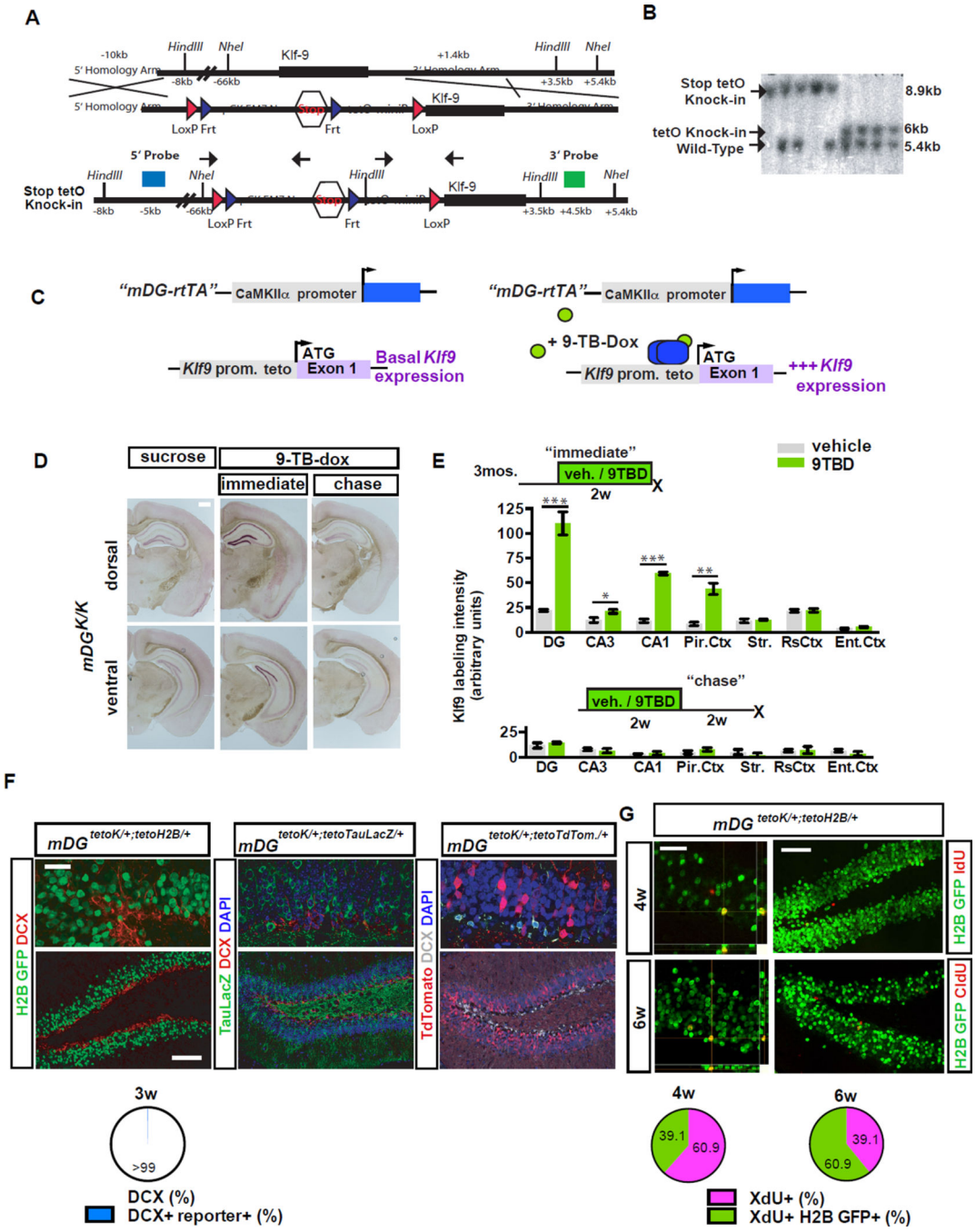

Figure 1. A genetic system for inducible and reversible overexpression of *Klf9* in mature DGCs

A) Strategy for targeting *Klf9* locus to generate *tetO-Klf9* knock-in mouse line.

B) Southern blot on F2 offspring DNA digested with *NheI* and probed with the 3' probe showing all 3 alleles (WT, Stop tetO-Knock-in, and TetO-Knock-in).

C-E) Inducible and reversible overexpression of *Klf-9*. (C) Schematic of tet-on genetic system. (D) In situ hybridization shows *Klf9* transcripts in $mDG^{K/K}$ mice are increased following two weeks of 9TBD treatment in drinking water (immediate) and are restored after

a two-week chase period. (E) Quantification of D (arbitrary units) at the immediate (top, n=5,3) and chase timepoint (n=3,3; bottom).

F) The *mDG rtTA* line drives expression in DGCs older than 3 weeks of age. Confocal images show absence of DCX and teto-reporter overlap in DGCs.

G) rtTA transactivates the *tetO-H2B GFP* transgene in DGCs 4 weeks of age and older. (n=3 mice). Scale bar: 500μm (D), 20μm top, 100μm below (F), 20μm top, 75μm below (G). For all figures data represent mean ± SEM unless otherwise noted and ***$p<0.001$, **$p<0.01$, *$p<0.05$.

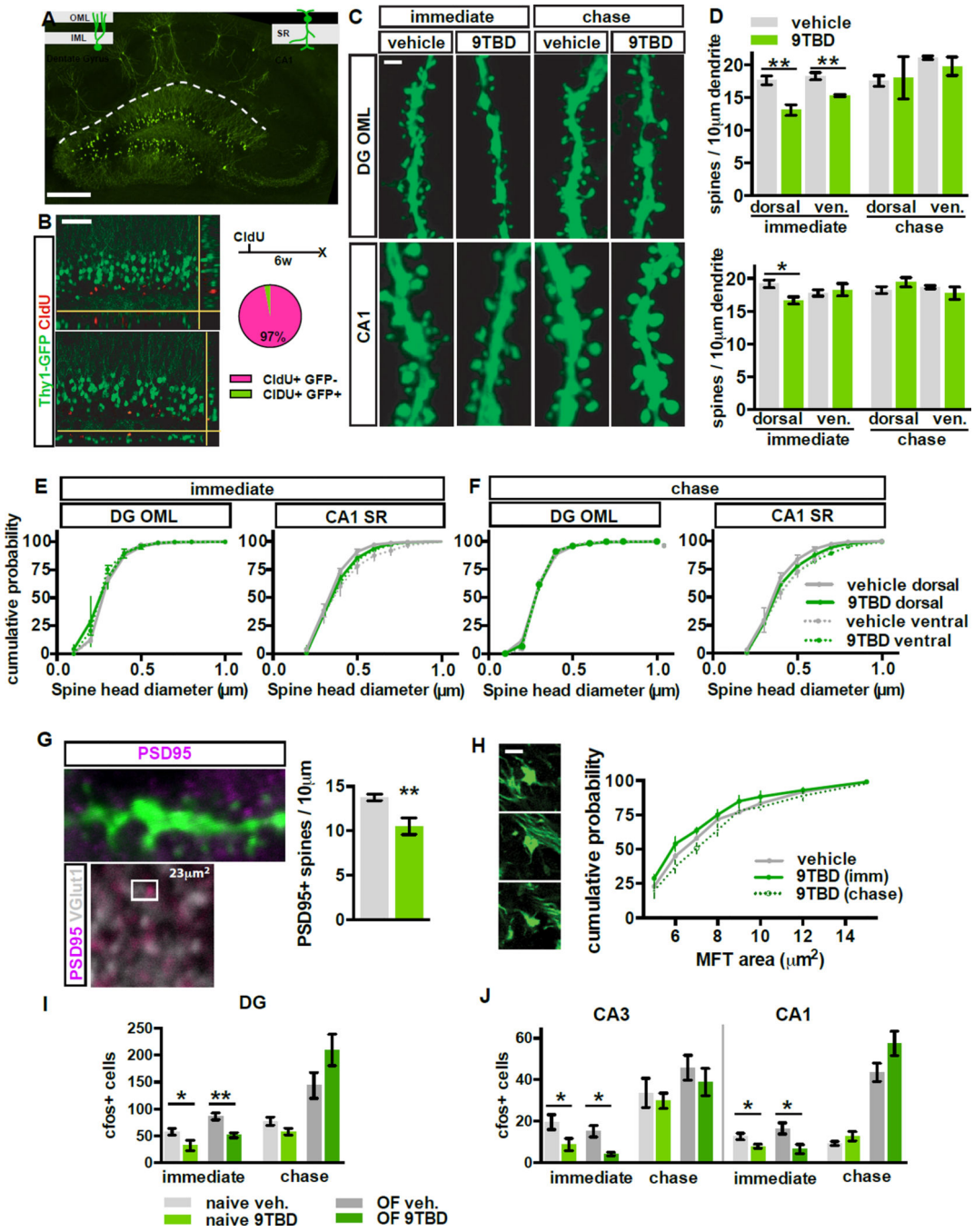

Figure 2. Reversible overexpression of *Klf9* transiently decreases dendritic spine density and activity of mature DGCs

A) GFP is expressed in a subset of DGCs and CA1 pyramidal neurons in *mDG*$^{K/K;Thy1\text{-}GFP(M)/+}$ mice. B) GFP+ DGCs in *mDG*$^{K/K;Thy1\text{-}GF(M)/+}$ are 6 weeks of age or older. Confocal scans of the GCL showing 6 week-old DGCs (CldU+) expressing GFP (arrowhead indicates overlap, n=3).

C,D) Inducible *Klf9* overexpression decreases dendritic spine density. (C) Maximum intensity projection confocal images of individual dendritic segments from OML (top) and

CA1-SR (below) at the immediate and chase timepoint in *mDG*$^{K/K;Thy1\text{-}GFP/+}$ mice. (D) Quantification of C (n=4,3).

E,F) The distribution of spine head diameter is unchanged in OML or SR of *mDG*$^{K/K;Thy1\text{-}GFP/+}$ mice (E) at the immediate (F) and chase timepoints (n=4,3 immediate, n=3,3 chase).

G) Inducible *Klf9* overexpression decreases the density of PSD95+ dendritic spines. Left, top: overlap between PSD95 and GFP-expressing dendrite. Left, below: representative image from DG OML showing adjacent opposing puncta of PSD95 and Vesicular glutamate transporter-1 (vGlut1). Right: quantification of PSD95+ dendritic spine density in the OML (n=3,5).

H) *Klf9* overexpression in mature DGCs does not affect MFT size. Graph displays the percentage distribution of MFT area (n=7[vehicle], 4[immediate], 3[chase]).

I, J) *Klf9* overexpression in mature DGCs transiently decreases the *cfos*+ population at (I) the immediate timepoint (home cage (n=7,7), 30 minutes of open field exploration (n=6,3)) but not the chase timepoint (home cage n=6,6, open field n=3,3). Scale bar: 500μm (A), 20μm (B), 2μm (C,G,H).

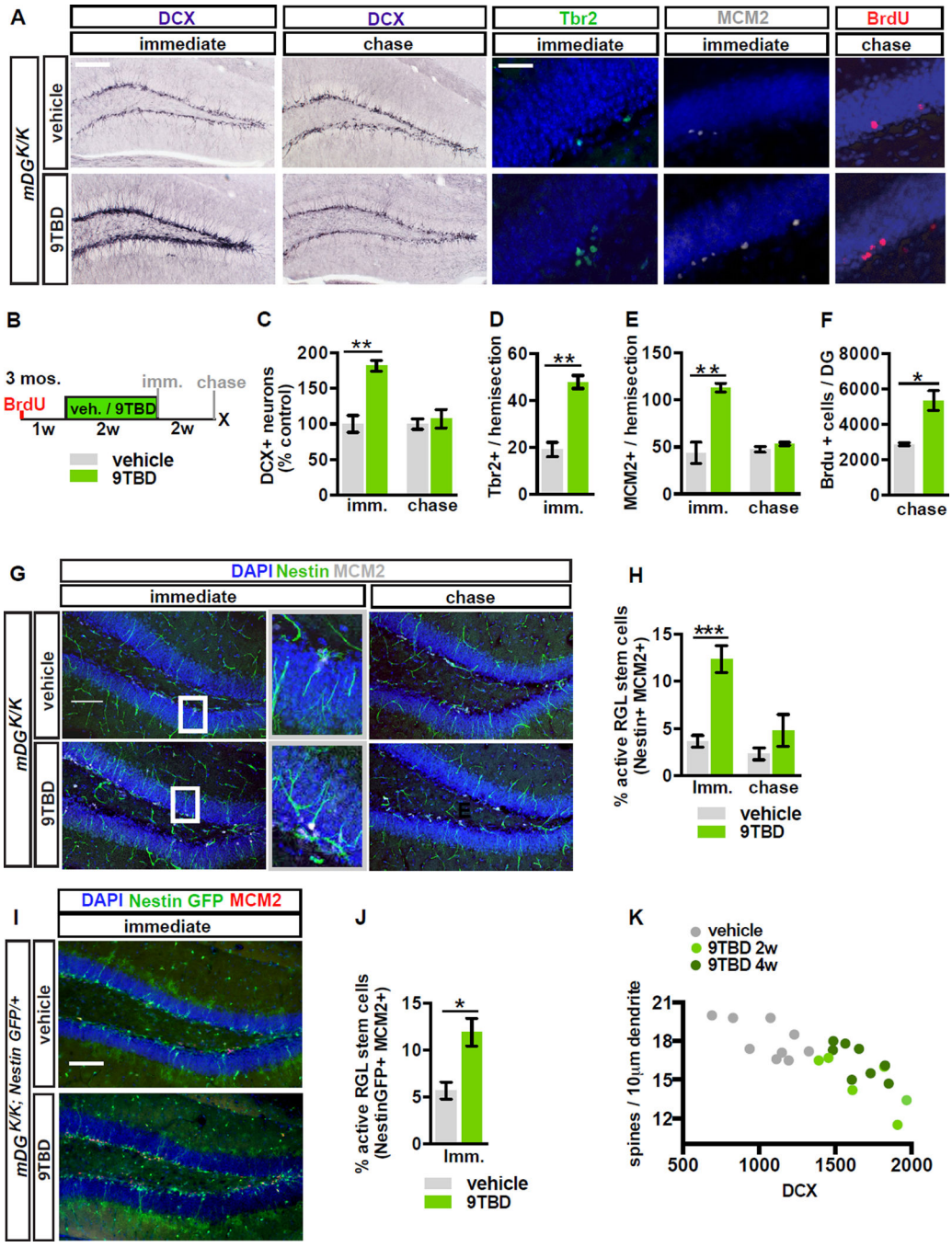

Figure 3. Reversible overexpression of *Klf9* in mature DGCs modulates activation of NSCs and neuronal competition dynamics

A - F) Adult hippocampal neurogenesis is reversibly enhanced in *mDG*$^{K/K}$ mice. (A) Images show labeling for DCX, Tbr2, MCM2, and BrdU. (B) Schematic indicates experimental design for Fig. 3A, C-J. (C) Reversible expansion of the DCX+ population in 9TBD treated *mDG* $^{K/K}$ mice (n=5,3 immediate, n=6,7 chase). (D) Increased number of progenitors (Tbr2+), (E) reversible enhancement of dividing cells (MCM2+) (n=3,3), and (F) enhanced survival of 5 week-old adult-born cells in GCL of 9TBD-treated *mDG*$^{K/K}$ mice (n=3,3).

G - J) NSC activation is reversibly enhanced in *mDG*$^{K/K}$ mice. (G) Representative images of activation of NSCs (arrowheads, Nestin+ MCM2+) with boxes to indicate magnified region. (H) Quantification of G (n=7,7). (I) Representative images of activated NSCs in vehicle and 9TBD-treated *mDG*$^{K/K;NestinGFP/+}$mice. (J) Quantification of I (n=3,4).

K) Dendritic spine density of mature DGCs is inversely correlated with the number of DCX + cells in dorsal DG. Dots represent individual animals. Scale bar: 100μm, 20 μm (A), 100μm (G,I).

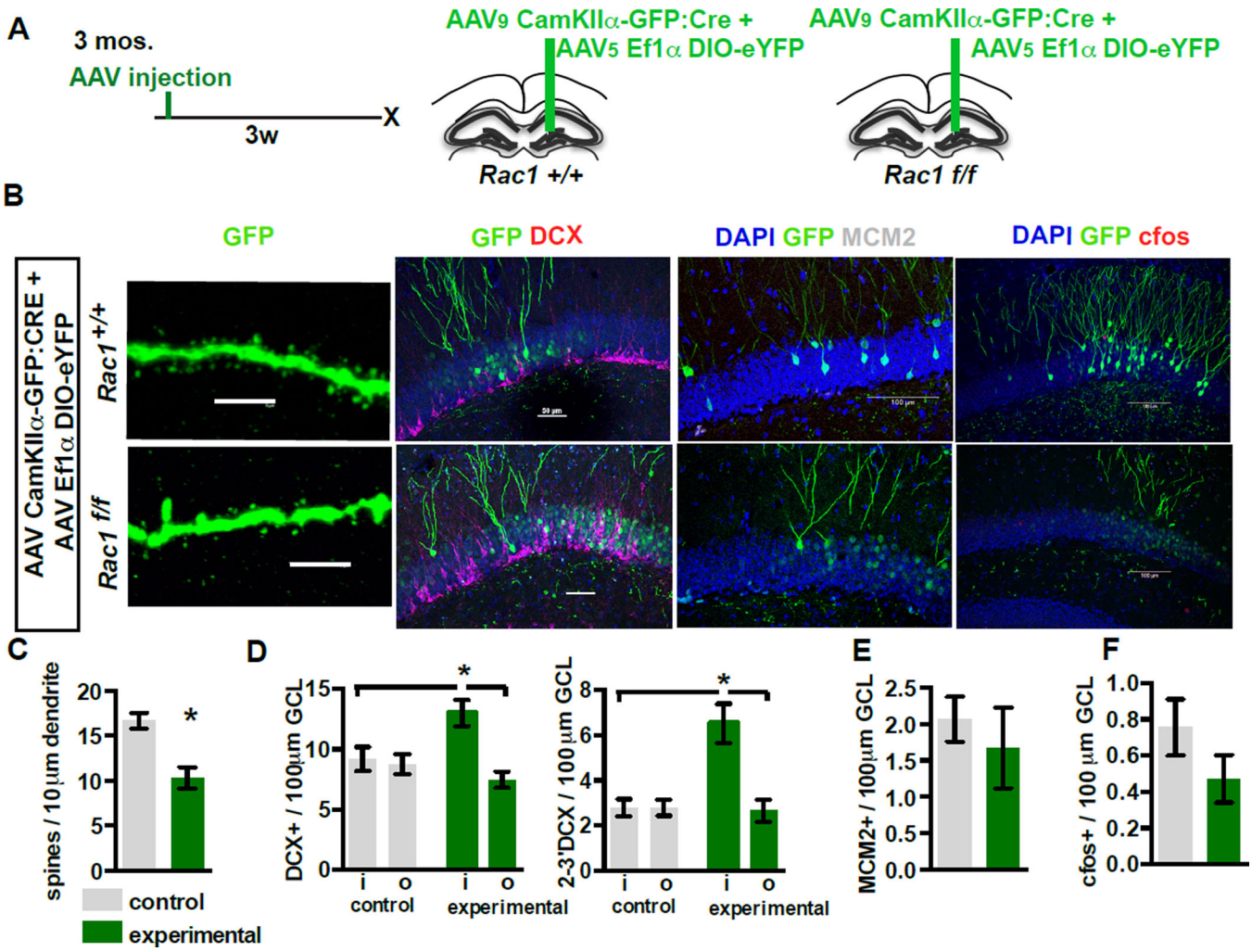

Figure 4. Conditional elimination of *Rac1* in mature DGCs decreases spine density and increases the survival of adult-born DGCs

A-D) Elimination of Rac1 expands the DCX+ population of adult-born DGCs. (A) Timeline and viral system. (B) Representative images of (left to right): OML dendritic segments, DCX, MCM2, and c-fos from Rac1 WT (top, AAV_9-CaMKIIα-Cre:GFP / AAV_8-EF1α-DIO-eYFP injected $Rac1^{+/+}$ animals) and Rac1 negative neurons (below, $Rac1^{f/f}$ animals) three weeks after virus infection (scale bars, left to right: 5μm, 50μm, 100μm, 100μm). (C) Inducible loss of *Rac1* reduces dendritic spine density (n=7,5). Control group also includes AAV_9-CaMKIIα-GFP / AAV_8-EF1α-DIO-eYFP injected $Rac1^{f/f}$ animals to control for potential genotype effects (n=4 of 7). (D) Inducible loss of *Rac1* increases the total DCX+ population (left) and the more mature DCX+ population (right) only in the area in which Cre virus is expressed in $Rac1^{f/f}$ animals.

E,F) Inducible loss of *Rac1* does not affect the MCM2+ population (E), or c-fos expression (F) in the virally transduced neurons (n=7,5)

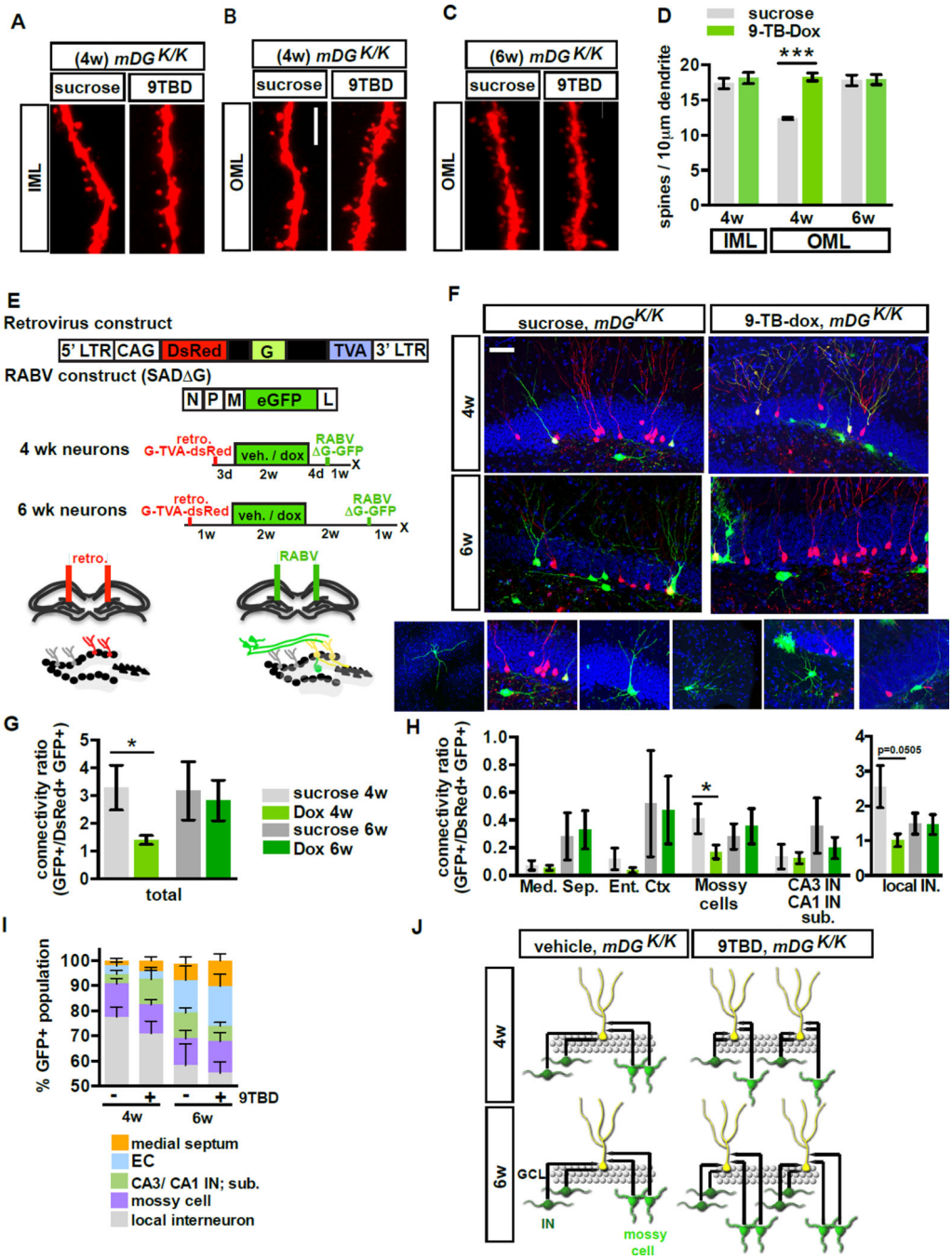

Figure 5. Genetic enhancement of adult hippocampal neurogenesis transiently reorganizes local afferent connectivity of maturing adult-born DGCs

A - D) 4 but not 6-week-old adult-born DGCs of 9TBD-treated *mDG*$^{K/K}$ mice have greater spine density than vehicle treated *mDG*$^{K/K}$ mice. (A, C) Maximum intensity projections of confocal z-stack scans of OML and (B) IML dendritic segments 4 weeks (A,B) or 6 weeks (C) after injection of DsRed-expressing retrovirus. 9TBD was administered as shown in Fig. 5E. (D) Quantification of A-C (4wk n=5,4, 6w n=3,3).

E - J) Decreased local monosynaptic inputs onto 4-week-old, but not 6-week-old, adult-born DGCs in 9TBD treated *mDG*$^{K/K}$ mice. (E) Schematic showing rabies virus constructs and

injection paradigm for F-J. (F) Representative images of dorsal DG sections showing retrovirally labeled cells (red), starter cells (yellow), and presynaptic partners (green). Below, images of specific presynaptic cell types. (G) Connectivity ratio of 4-week, but not 6-week-old, adult-born DGCs is decreased in 9TBD-treated $mDG^{K/K}$mice relative to controls (n=4 for all groups) with (H) specific reductions in connectivity to mossy cells and interneurons (n=4 DG INs p=0.0505). (I) 4 and 6-week-old adult-born DGCs of vehicle and 9TBD treated $mDG^{K/K}$ show similar distributions of pre-synaptic cells. (J) Population-level model conveying how enhancing adult hippocampal neurogenesis reorganizes inputs from mossy cells and DG INs. Scale bar: 5μm (A,C), 20 μm (F).

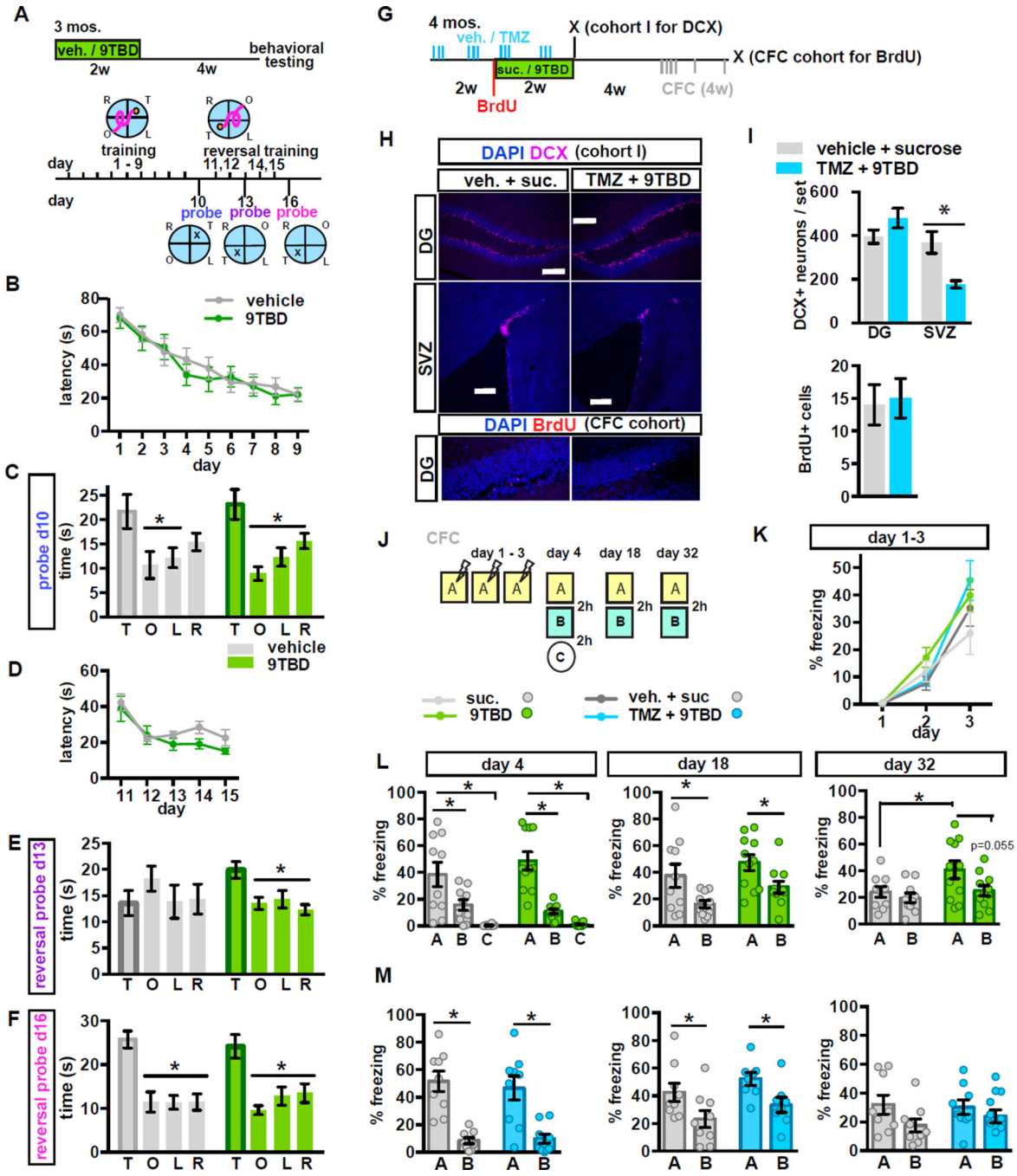

Figure 6. Genetic expansion of a cohort of 5–8 week-old adult-born DGCs decreases spatial interference and enhances long-term memory strength and precision

A - F) (A) Schematic of MWM paradigm used in B-F. (B) Vehicle and 9TBD treated *mDG*$^{K/K}$ mice exhibit similar latencies to locate the hidden platform across training days (n=10,10). (C) Both groups preferred the target quadrant during the probe trial on day 10. (D) Vehicle and 9TBD-treated *mDG*$^{K/K}$ mice exhibit similar latencies to locate the hidden platform during training at the reversal location. (E) In the first reversal probe (day 13 prior to training) 9TBD-treated *mDG*$^{K/K}$ mice, but not controls, spent significantly more time in

the target quadrant whereas (F) both groups spent similar amounts of time swimming in the target quadrant during the probe trial on day 16.

G-I) Concurrent TMZ treatment prevents the KLF9 overexpression-induced expansion of the adult-born neuron population. (G) Schematic of TMZ and 9TBD dosing used for H,I, K, M (H) Representative images show no change in the DCX+ population of adult-born DGCs, but a reduction in DCX+ adult-born neurons in the SVZ in TMZ/9TBD treated $mDG^{K/K}$ mice. Scale bars 200mm. Below, representative images of BrdU labeling as described in I. (I) Above: In the DG, TMZ treatment prevents the KLF9 overexpression-induced increase in neurogenesis (n=4), and in the SVZ, where *Klf9* overexpression does not affect neurogenesis, TMZ treatment significantly reduced neurogenesis (n=4,5). Below: Quantification of DG BrdU+ cells shows no change. BrdU was given at the start of 9TBD or sucrose treatment (i.e. halfway through the vehicle or TMZ treatment paradigm) and animals were sacrificed after CFC testing was completed (n=4,4).

J - M) Expansion of the 5–8-week-old adult-born DGC population improves memory precision. (J) Schematic of the contextual fear conditioning paradigm. (K) Vehicle and 9TBD-treated (n=10,11), and vehicle/sucrose and TMZ/9TBD treated (n=8,8) $mDG^{K/K}$ mice exhibited comparable acquisition of contextual fear memory over 3 days. (L) 9TBD-treated $mDG^{K/K}$ mice exhibited modestly improved discrimination of similar contexts at day 32 (t-test, A vs. B, 9TBD: p=0.0546) and enhanced long-term contextual fear memory at day 32 (t-test, vehicle A vs. 9TBD A: p=0.0495). (M) Vehicle/sucrose and TMZ/9TBD treated $mDG^{K/K}$ mice showed no differences in discrimination at day 4, 18, or 32. For CFC data, graphs show mean ± SEM with individual animals shown as circles.

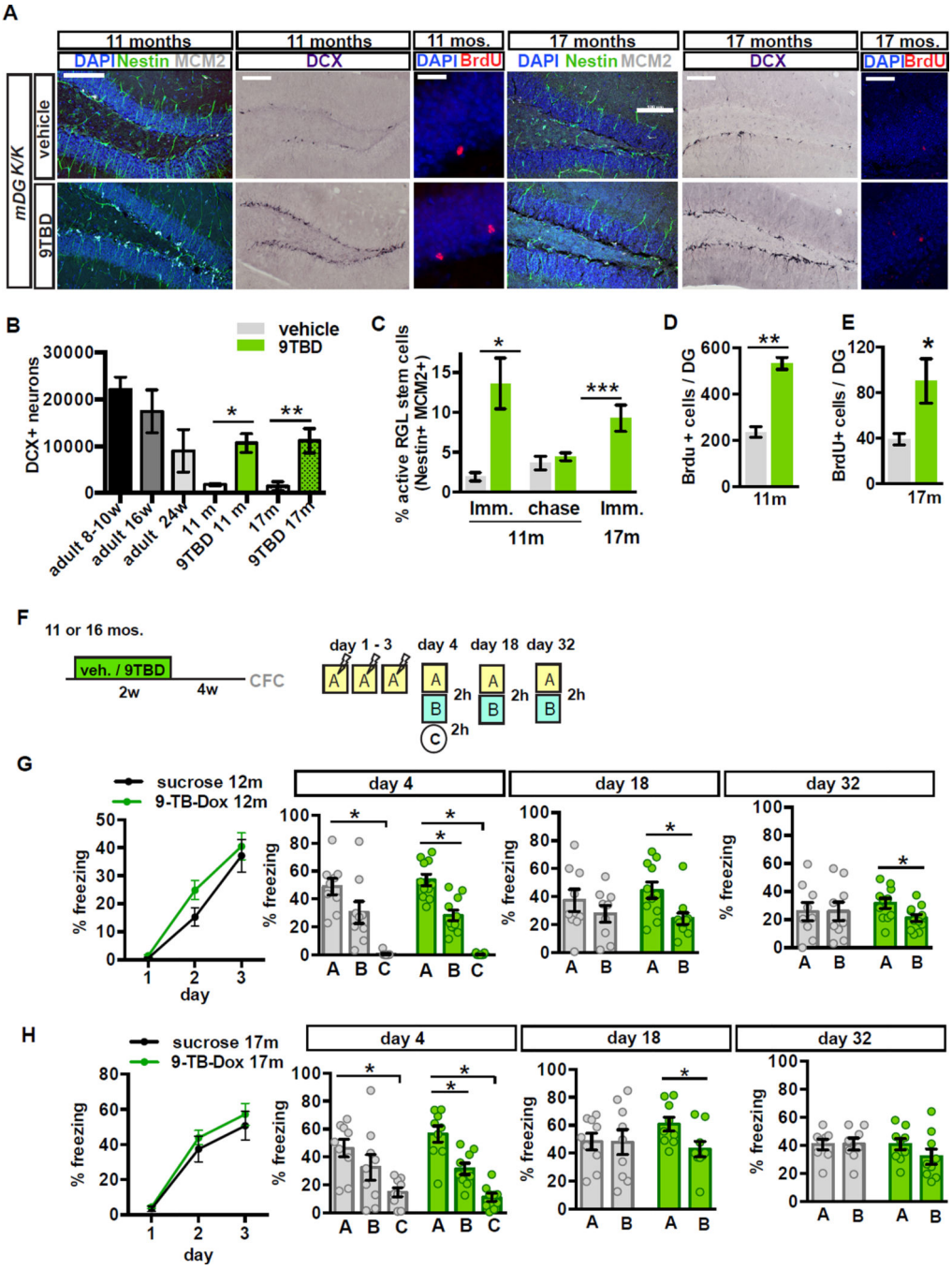

Figure 7. Contextual memory precision is improved in middle-aged and aged mice with expanded populations of 5–8 week-old adult-born DGCs

A - D) Enhancement of adult hippocampal neurogenesis in middle-aged and aged *mDG*$^{K/K}$ mice. (A) Representative hippocampal images from 11 and 17-month-old vehicle or 9TBD-treated *mDG*$^{K/K}$ mice showing labeling for DCX, Nestin and MCM2 (activated NSCs), and BrdU. (B) The DCX+ population is increased in 9TBD-treated *mDG*$^{K/K}$ mice at 11 months (10667±2011) and 17 months old (11160±1286) to levels comparable to that of 5–6-month-old mice (9000±2266)(11m n=3,4, 17m: n=4,4) (C, D). Enhanced (C) activation of NSCs

and (D) survival of 3 week-old adult-born cells in 9TBD-treated 11 and 17-month-old $mDG^{K/K}$ mice (11m n=3,4, 17m n=3,3 for survival n=4,4).

F - H) 12 and 17-month-old mice with expanded populations of adult-born neurons show modest enhancements in a contextual fear conditioning task. (F) Schematic of the CFC paradigm used in G, H (12m n=8,10, 17m n=9,9). (G) 12 month-old $mDG^{K/K}$ mice with an expanded population of 5–8 week-old adult-born DGCs exhibit discrimination of similar contexts at day 4, day 18 and day 32. (H) 17-month-old $mDG^{K/K}$ mice with expanded population of 5–8 week-old adult-born DGCs exhibit discrimination of similar contexts at day 4 and day 18 but not day 32. Scale bar: 20 μm (BrdU) 100μm (remainder) (A).

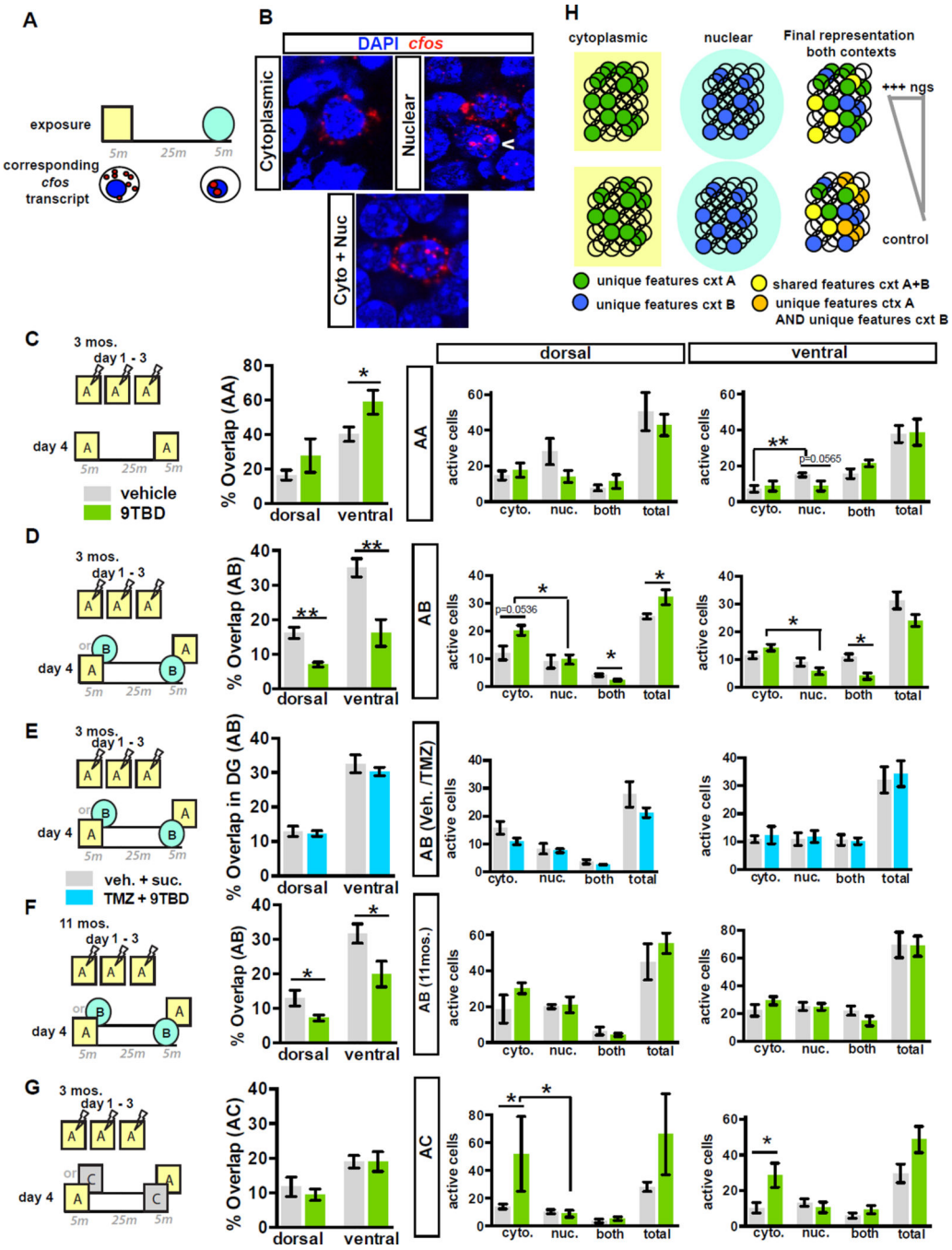

Figure 8. Expansion of a cohort of 5–8 week-old adult-born DGCs enhances global remapping in the DG

A) Schematic outlining catFISH concept using *c-fos* intronic and full-length cDNA probes as utilized in B– G.

B) DGCs exhibiting cytoplasmic, nuclear, or nuclear and cytoplasmic localization of *c-fos* transcripts.

C) Expanding the cohort of 5–8 week-old adult-born DGCs enhances reactivation of DG cellular assemblies in ventral DG following repeat exposure to the same context (ventral A-A, n=6,4). Both groups of mice showed similar numbers of active cells (Right).

D - F) Expansion of a cohort of 5–8 week-old adult-born DGCs (E, n=6,6), significantly decreases reactivation of cellular assemblies in dorsal and ventral DG following exposure to similar contexts (A–B) in adult (D) (n=7,4) and middle-aged (F) (n=4,5) mice. In adult mice, this expansion increases active cells following first exposure and increases sparseness following second exposure (D, Right).

G) Genetic expansion of a cohort of 5–8 week-old adult-born DGCs does not affect global remapping in DG in response to a distinct context (n=6,3) although the population of active cells following the first exposure is increased (Right).

H) Model: Increasing neurogenesis increases the pool of adult-born DGCs re-activated by features common to both contexts (yellow circles). This in turn decreases the likelihood of re-activating DGCs used to encode unique features of previously experienced contexts (orange circles), thereby decreasing overlap between engrams of contexts A and B.